

INVESTIGATING OBJECT COMPOSITIONALITY IN GENERATIVE ADVERSARIAL NETWORKS*

Sjoerd van Steenkiste^{†,1}, Karol Kurach², Jürgen Schmidhuber^{1,3}, Sylvain Gelly²

¹ IDSIA, USI, SUPSI, ² Google Brain, ³ NNAISENSE

ABSTRACT

Deep generative models seek to recover the process with which the observed data was generated. They may be used to synthesize new samples or to subsequently extract representations. Successful approaches in the domain of images are driven by several core inductive biases. However, a bias to account for the compositional way in which humans structure a visual scene in terms of objects has frequently been overlooked. In this work, we investigate object compositionality as an inductive bias for Generative Adversarial Networks (GANs). We present a minimal modification of a standard generator to incorporate this inductive bias and find that it reliably learns to generate images as compositions of objects. Using this general design as a backbone, we then propose two useful extensions to incorporate dependencies among objects and background. We extensively evaluate our approach on several multi-object image datasets and highlight the merits of incorporating structure for representation learning purposes. In particular, we find that our structured GANs are better at generating multi-object images that are more faithful to the reference distribution. More so, we demonstrate how, by leveraging the structure of the learned generative process, one can ‘invert’ the learned generative model to perform unsupervised instance segmentation. On the challenging CLEVR dataset, it is shown how our approach is able to improve over other recent purely unsupervised object-centric approaches to image generation.

1 INTRODUCTION

Probabilistic generative models aim to recover the process with which the observed data was generated. It is postulated that knowledge about the generative process exposes important factors of variation in the environment (modeled by latent variables) that may subsequently be obtained using an appropriate posterior inference procedure. Hence, in order to use generative models for representation learning, it is important that the *structure* of the generative model closely resembles the underlying generative process.

Deep generative models of images rely on the expressiveness of neural networks to learn the generative process directly from data (Goodfellow et al., 2014; Kingma & Welling, 2014; Van Oord et al., 2016).

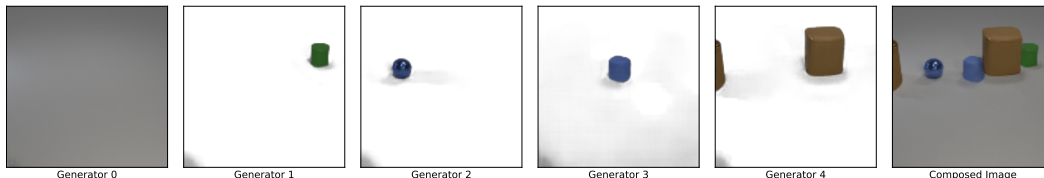


Figure 1: In this paper, we investigate three simple modifications to a neural network generator that allows it to generate images as a composition of a generated background (left) and generated individual objects (middle). The resulting generated image is shown on the right.

*A preliminary version (van Steenkiste et al., 2018b) of this work appeared under a different title as a workshop paper at NeurIPS 2018 and as a technical report on arXiv (v1).

[†]The majority of this work was done while at Google Brain. Correspondence to sjoerd@idsia.ch.

Their structure is determined by the *inductive bias* of the neural network, which steers it to organize its computation in a way that allows salient features to be recovered and ultimately captured in a representation (Kingma & Welling, 2014; Dinh et al., 2017; Donahue et al., 2017; Dumoulin et al., 2017). Recently, it was shown that independent factors of variation, such as pose and lighting of human faces may be recovered in this way (Chen et al., 2016; Higgins et al., 2017).

A promising, but under-explored, inductive bias in deep generative models of images is *compositionality at the representational level of objects*, which accounts for the compositional nature of the visual world and our perception thereof (Spelke & Kinzler, 2007; Battaglia et al., 2013). It allows a generative model to describe a scene as a composition of objects, thereby ‘disentangling’ visual information that can be processed largely independently of one another. By explicitly accounting for object compositionality one imposes an *invariance* that simplifies the generative process, and potentially allows one to (more efficiently) learn a more accurate generative model of images. Moreover, by explicitly considering individual objects at a representational level, (posterior) inference in the learned generative model allows one to recover corresponding object representations that are desirable for many ‘down-stream’ learning tasks (Santoro et al., 2017; Janner et al., 2019).

In this work, we investigate object compositionality for Generative Adversarial Networks (GANs) (Goodfellow et al., 2014)¹. We investigate a minimal modification to a standard neural network generator that incorporates the right inductive bias and find that it reliably learns to generate images as compositions of objects. Using this general design as a backbone, we then propose two useful extensions that provide a means to incorporate dependencies among objects and background in the generative process. Finally, we demonstrate how one can leverage the learned structured generative process, which is now interpretable and semantically understood, to perform inference and recover individual objects from multi-object images without additional supervision.

The goal of this work is not to improve upon state-of-the-art approaches to multi-object image generation that rely on prior knowledge by *conditioning* on explicit scene graphs (Johnson et al., 2018; Xu et al., 2018), images of individual objects (Lin et al., 2018; Azadi et al., 2019), or their properties (Hinz et al., 2019). Rather, we suggest an alternative approach to learn deep generative models for complex visual scenes based on GANs, that does not rely on prior knowledge in the form of conditioning. Instead, our approach *learns* to separate information about objects at a representation level, so that it can be ‘inverted’ to extract this knowledge. As a consequence, without relying on prior knowledge in the form of auxiliary inputs that are generally not available, the approach presented here contributes an important step in developing purely unsupervised generative models for representation learning purposes that are expected to be more applicable in the context of AI (Bengio et al., 2013).

We extensively evaluate our structured generator² on several multi-object image datasets. When using our inductive bias, we find that GANs are able to learn about the individual objects and the background of a scene, without prior access to this information (Figure 1). The results of our quantitative experiments highlight the merits of incorporating these inductive biases for representation learning purposes. In particular, compared to a strong baseline of popular GANs including recent state-of-the-art techniques, our approach consistently outperforms in generating better images that are more faithful to the reference distribution. More so, we demonstrate how, by leveraging the structure of the learned generative process, one can perform inference in these models and perform unsupervised instance segmentation. On the challenging CLEVR dataset (Johnson et al., 2017) it is shown how our approach is able to improve over other recent purely unsupervised object-centric approaches to image generation.

2 GENERATIVE ADVERSARIAL NETWORKS

Generative Adversarial Networks (GANs) are powerful generative models that learn a stochastic procedure to generate samples from a distribution $P(X)$. Traditionally GANs consist of two deterministic functions: a generator $G(z)$ and a discriminator (or critic) $D(x)$. The goal is to find a generator that accurately transforms samples from a prior distribution $z \sim P(Z)$ to match samples from the target distribution $x \sim P(X)$. This can be done by using the discriminator to implement

¹There exist interesting parallels between GANs and earlier approaches (Schmidhuber, 1990; 1992), and we refer the reader to Schmidhuber (2020) for a comparison.

²Code is available online at <https://git.io/JePuK>.

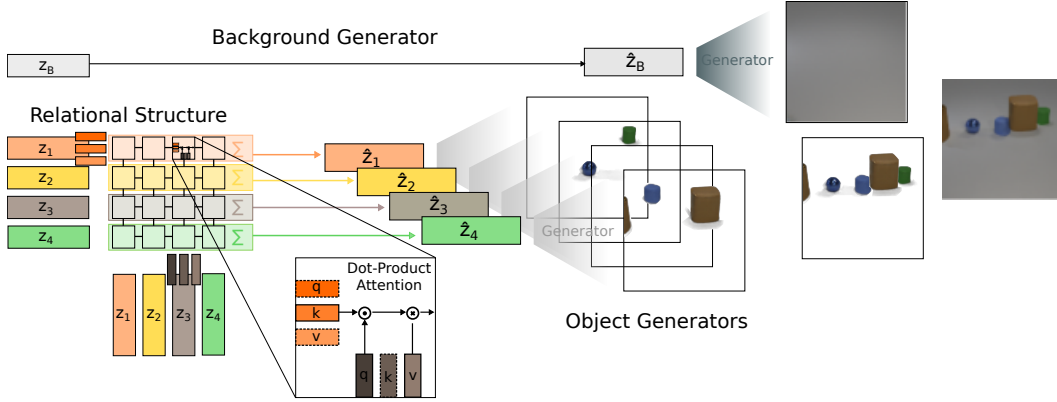


Figure 2: We propose three modifications to a standard neural network generator to generate images as a composition of individual objects and background. In this case, it consists of $K = 4$ *object generators* (shared weights) that each generate an image from separate latent vector $z_i \sim P(Z)$, which serve as the backbone for object compositionality. On the left side, a *relational stage* is shown as one possible extension to model relations between objects by first computing \hat{z}_i from z_i that are then fed to the object generators. In the back, a second extension is shown that incorporates a *background generator* (unique weights) to generate a background image from a separate latent vector $z_b \sim P(Z_b)$. The whole system is trained end-to-end as in the standard GAN framework, and the final image is obtained by composing (in this case using alpha compositing) the outputs of all generators.

a suitable objective for the generator, in which it should behave *adversarially* with respect to the goal of the discriminator in determining whether samples x were sampled from $P(X)$ or $G(P(Z))$ respectively. These objectives can be summarized as a *minimax* game with the following value function:

$$\min_G \max_D V(D, G) = \mathbb{E}_{x \sim P(X)} [\log D(x)] + \mathbb{E}_{z \sim P(Z)} [\log(1 - D(G(z)))] . \quad (1)$$

When the generator and the discriminator are implemented with neural networks, optimization may proceed through alternating (stochastic) gradient descent updates of their parameters with respect to (1). However, in practice, this procedure might be unstable and the minimax formulation is known to be hard to optimize. Many alternative formulations have been proposed and we refer the reader to Lucic et al. (2018) and Kurach et al. (2019) for a comparison.

Based on the findings of Kurach et al. (2019) we consider two practical reformulations of (1) in this paper: Non-Saturating GAN (NS-GAN) (Goodfellow et al., 2014), in which the generator maximizes the probability of generated samples being real, and Wasserstein GAN (WGAN) (Arjovsky et al., 2017) in which the discriminator minimizes the Wasserstein distance between $G(P(Z))$ and $P(X)$. In both cases, we explore two additional techniques that have proven to work best on a variety of datasets and architectures: the gradient penalty from Gulrajani et al. (2017) to regularize the discriminator, and spectral normalization (Miyato et al., 2018) to normalize its gradients.

3 INCORPORATING STRUCTURE

In order to formulate the *structure* (inductive bias) required to achieve object compositionality in neural network generators, we will focus on the corresponding type of invariance that we are interested in. It is concerned with independently varying the different objects that an image is composed of, which requires these to be identified at a representational level and described in a common format.

In the following subsections, we first present a simple modification to a neural network generator to obtain object compositionality. Afterward, we present two useful extensions that allow one to additionally reason about relations between objects, and to model background and occlusions.

3.1 OBJECT COMPOSITIONALITY

A minimal modification of a neural network generator assumes that images $\mathbf{x} \sim P(X)$ are composed of objects that are independent of one another. For images having K objects, we consider K i.i.d. vector-valued random variables Z_i that each describe an object at a representational level. K copies of a deterministic generator $G(\mathbf{z})$ transform samples from each Z_i into images, such that their superposition results in the corresponding output image:

$$\mathbf{x} = \sum_{i=1}^K G(\mathbf{z}_i), \text{ where } \mathbf{z}_i \sim P(Z). \quad (2)$$

When each copy of G generates an image of a single object, the resulting generative model efficiently generates images in a compositional manner (Figure 3). Each object in (2) is described in terms of the same features (i.e. the Z_i 's are i.i.d) and the weights among the generators are shared, such that any acquired knowledge in generating a specific object is transferred across all others. Hence, rather than having to learn about all combinations of objects (including their own variations) that may appear in an image, it suffices to learn about the different variations of each individual object. This greatly simplifies the generative process without losing generality.

The superposition of generators in (2) can be viewed as a single generator of the form $G_{multi}(\mathbf{z} = [\mathbf{z}_1, \dots, \mathbf{z}_K])$ and trained as before using the objective in (1). The generators in (2) do not interact, which prevents degenerate solutions and encourages G to learn about objects. However, it also implies that relations between objects *within* a scene cannot be modelled in this way. Finally, we note that the sum in (2) assumes that images only consist of objects, and that their values can be summed in pixel-space. We will now present two extensions that focus on each of these aspects and incorporate additional structure besides the superposition of generators that serves as the basis for object compositionality.

3.2 RELATIONS BETWEEN OBJECTS

In the real world, objects are not strictly independent of one another. Certain objects may only occur in the presence of others, or affect their visual appearance in subtle ways (eg. shadows). In order to facilitate relationships of this kind our first extension consists of a *relational stage*, in which the representation of an object is updated as a function of all others, before each generator proceeds to generate its image.

The relational stage is a *graph network* which, in our case, consists of one or more self-attention blocks that compute these updates. At the core of each attention block is Multi-Head Dot-Product Attention (MHDP) (Vaswani et al., 2017) that performs message-passing when one associates each object representation with a node in a graph (Battaglia et al., 2018). This is a natural choice since it was shown that relations between objects and corresponding updates to their representations can be learned efficiently in this way (Zambaldi et al., 2019).

Similar to Zambaldi et al. (2019), a single head of an attention block first projects each latent vector \mathbf{z}_i (associated with an object) into so-called query, key, and value vectors:³

$$\mathbf{q}_i = \text{MLP}^{(q)}(\mathbf{z}_i), \quad \mathbf{k}_i = \text{MLP}^{(k)}(\mathbf{z}_i), \quad \mathbf{v}_i = \text{MLP}^{(v)}(\mathbf{z}_i). \quad (3)$$

Next, the interaction of an object i with all other objects (including itself) is computed as a weighted sum of their value vectors. Weights are determined by computing dot-products between its query vector and all key vectors, followed by softmax normalization:

$$\mathbf{A} = \underbrace{\text{softmax}(\mathbf{Q}\mathbf{K}^T/\sqrt{d})}_{\text{attention weights}} \mathbf{V}, \quad (4)$$

³The role of the key and value vectors are analogous to those in a key-value database. However, in this case access takes place on the basis of similarity between key and query vectors (i.e. the attention weights), which allows this process to be differentiated.

where $d = \dim(\mathbf{v}_i)$ and $\mathbf{K}, \mathbf{Q}, \mathbf{V} \in \mathbb{R}^{K \times d}$ are matrices that contain the key, query, and value vectors for each object. $\mathbf{A} \in \mathbb{R}^{K \times d}$ contains the result of each object attending to all other representations. Finally, we proceed by projecting each update vector \mathbf{a}_i back to the original size of \mathbf{z}_i before being added:

$$\hat{\mathbf{z}}_i = \text{MLP}^{(u)}(\mathbf{a}_i) + \mathbf{z}_i. \quad (5)$$

Additional heads (modeling different interactions) use different parameters for each MLP, and their outputs are combined with another MLP to arrive at a final $\hat{\mathbf{z}}_i$. Complex relationships among objects can be modeled by using multiple attention blocks to *iteratively* update \mathbf{z}_i . A detailed overview of these computations can be found in B and a schematic in Figure 2.

3.3 BACKGROUND AND OCCLUSION

The second extension that we propose explicitly distinguishes the background from objects. Complex visual scenes often contain visual information that only appears in the background and does not occur frequently enough (or lacks a regular visual appearance) to be modeled as objects. Indeed, one assumption that we have made is that objects can be compactly encoded in a representation \mathbf{z}_i that is described in a *common format*. Treating background as an “extra” object violates this assumption as the latent representations \mathbf{z}_i (and corresponding generator) now need to describe objects that assume a regular visual appearance, as well as the background that is not regular in its visual appearance at all. Therefore, we consider an additional *background* generator (see Figure 2) having its own set of weights to generate the background from a separate vector of latent variables $\mathbf{z}_b \sim P(Z_b)$. We will explore two different variations of this addition, one in which \mathbf{z}_b participates in the relational stage, and one in which it does not.

A remaining challenge is then in *combining* objects with background and in modeling occlusion. A straightforward adaptation of the sum in (2) to incorporate pixel-level weights would require the background generator to assign a weight of zero to all pixel locations where objects appear, thereby increasing the complexity of generating the background exponentially. Instead, we require the object generators to generate an additional alpha channel for each pixel (while treating the output of the background generator as opaque), and use alpha compositing to combine the K different outputs of the object generators (\mathbf{x}_i, α_i) and background generator $(\mathbf{x}_b, 1)$ as follows:

$$\mathbf{x} = \sum_{i=1}^K \left[\mathbf{x}_i \alpha_i \prod_{j=1}^{i-1} (1 - \alpha_j) \right] + \mathbf{x}_b \prod_{i=1}^K (1 - \alpha_i). \quad (6)$$

Using alpha compositing as in (6) is a standard technique in computer graphics, and therefore a natural choice in generating images. On the other hand, alpha compositing uses a fixed ordering that assumes that the generated images (when overlapping) are provided in the correct order. In principle, the relational stage can ensure that this is the case, although it may be difficult to learn in an adversarial setting. An alternative choice would be to *learn* to composite, for example by using a conditional GAN that starts from images of individual objects (Lin et al., 2018; Azadi et al., 2019). Here, we opt for the simpler choice of using (6) as we are primarily concerned with investigating the possibility of learning to generate images in this way.

4 RELATED WORK

Prior works on incorporating inductive biases aimed at object compositionality typically treat an image as a *spatial mixture* of image patches and utilizes multiple copies of the same function to arrive at a compositional solution. Different implementations use RBMs (Le Roux et al., 2011), VAEs (Nash et al., 2017), or (recurrent) auto-encoders inspired by EM-like inference procedures (Greff et al., 2016; 2017) to generate these patches. It was also shown that interactions between objects can be modeled efficiently in this way (van Steenkiste et al., 2018a). Neither of these works has shown to be capable of generating more complex visual scenes that incorporate unstructured background as well as relations between objects. By observing that GANs are often superior in terms of image generation capabilities, and by adding structure, we are able to improve upon these works in this regard. Indeed,

compared to the recent IODINE (Greff et al., 2019) that also utilizes a spatial mixture formulation, we will demonstrate how our approach better succeeds at modeling complex image distributions.

A conceptually similar line of related work uses variational inference to learn recurrent neural networks to *iteratively* generate an image, one patch at a time (Gregor et al., 2015; Eslami et al., 2016; Kosiorek et al., 2018). The work by Eslami et al. (2016) incorporates a strong inductive bias that associates each image patch with a single object. However, also their approach is limited to generating (sequences) of binary images without background (Eslami et al., 2016; Kosiorek et al., 2018). Related settings have also been explored with GANs using a recurrent generator (Im et al., 2016; Kwak & Zhang, 2016), while other work (Yang et al., 2017) additionally considers a separate generator for the background that uses spatial transformations to integrate a foreground image. From these, only the work of Yang et al. (2017) briefly explores the problem of multi-object image generation on a dataset consisting of two non-overlapping MNIST digits. Their approach is only moderately successful while making extra assumptions about the size of the digits. Importantly, their approach does not provide a means to ‘invert’ the learned model and perform inference.

Other recent work in GANs has focused on *conditional* image generation to simplify the task of multi-object image generation. Johnson et al. (2018) generate multi-object images from explicit scene graphs, while Xu et al. (2018) condition on a stochastic and-or graph instead. Azadi et al. (2019) propose a framework to generate images composed of two objects by combining the images of each individual object. Similarly, Lin et al. (2018) present an iterative scheme to remove or add objects to a scene based on prior knowledge about individual objects. Hinz et al. (2019) require object labels and bounding boxes to generate complex visual scenes consisting of multiple objects and background. While these works generate realistic multi-object scenes, they require prior information (scene graphs, segmentations, etc.) about individual objects or scenes that is typically not available in many real-world settings. Our work serves a complementary purpose in terms of image generation in that regard: while we consider visually simpler scenes, we do not require any extra information about scenes or objects. In the context of representation learning, we are also able to ‘invert’ the learned generative model by leveraging its structure to learn about objects. This sets us firmly apart from these methods and also from standard unstructured GANs that do not rely on conditioning. Indeed, without explicitly considering objects at a representational level (requiring architectural structure), one is unable to recover individual objects in this way.

In the context of unsupervised instance segmentation, three very recent works propose to structure the generator of a GAN to directly learn to perform instance segmentation. The copy-paste GAN from Arandjelović & Zisserman (2019) uses a generator to generate a mask that interpolates between two images and learns to discover objects. Chen et al. (2019) decompose the generative process in a segmentation step that separates foreground and background, and a generation step that in-paints the foreground segment. Finally, Bielski & Favaro (2019) present a layered generator that distinguishes between foreground and background by perturbing the foreground image relative to the background. Our approach is different insofar we present a structured generator that facilitates *both* generation and segmentation of visual scenes that are composed of multiple objects and background, and which is trained purely for generation purposes.

5 EXPERIMENTS

We investigate different aspects of the proposed structure on several multi-object datasets. We are particularly interested in verifying that images are generated as compositions of objects and that the relational and background structure is properly utilized. Moreover, we study how the incorporated structure affects the quality of the generated images, and how it may be used to perform inference in the form of instance segmentation.

Datasets We consider five multi-object datasets⁴. The first three are different variations of *Multi-MNIST (MM)*, in which each image consists of three MNIST digits (LeCun et al., 1998) that were rescaled and drawn randomly onto a 64×64 canvas. In *Independent MM*, digits are chosen randomly and there is no relation among them. The *Triplet* variation imposes that all digits in an image are of the same type, requiring relations among the digits to be considered during the generative process. Similarly in *RGB Occluded MM* each image consists of exactly one red, green, and blue digit. The

⁴Datasets are available online at <https://goo.gl/Eub81x>.

fourth dataset (*CIFAR10 + MM*) is a variation of CIFAR10 (Krizhevsky et al., 2009) in which the digits from *RGB Occluded MM* are drawn onto a randomly chosen (resized) CIFAR10 image. Our final dataset is *CLEVR* (Johnson et al., 2017), which we downsample to 160×240 followed by center-cropping to obtain 128×128 images. Samples from each dataset can be seen in C.

Evaluation A popular evaluation metric to evaluate GANs is the Fréchet Inception Distance (FID) (Heusel et al., 2017). It computes the distance between two empirical distributions of images as the Fréchet distance between two corresponding multivariate Gaussian distributions that were estimated using the features of a pre-trained Inception network for each image. Although prior work found that FID correlates well with perceived human quality of images on standard image datasets (Lucic et al., 2018), we find that FID is less useful when considering images consisting of *multiple* salient objects. Our results in Section 5.2 suggest that FID is not a good indicator of performance during later stages of training, and may easily be fooled by a GAN that focuses on image statistics rather than content (e.g. generating the correct number of objects). We hypothesize that this inability is due to the Inception network having been trained only for single object classification.

Therefore, in addition to FID, we conduct two different studies among humans, 1) to compare images generated by our models to a baseline, and 2) to answer questions about the content of generated images. The latter allows us to verify whether generated images are probable samples from the true image distribution. As conducting a human evaluation of this kind is not feasible for large-scale hyper-parameter search, we will continue to rely on FID to select the “best” models during hyper-parameter selection. Details of these human studies can be found in B.

Set-up The GAN-based models are optimized with ADAM (Kingma & Ba, 2015) using a learning rate of 10^{-4} , and batch size 64 for 1M steps. We compute the FID (using 10K samples) every 20K steps, and select the best set of parameters accordingly. On each dataset, we compare GANs that incorporate our proposed structure to a strong baseline that does not. In both cases we conduct extensive grid searches covering on the order of 40-50 hyperparameter configurations for each dataset, using ranges that were previously found good for GANs (Lucic et al., 2018; Kurach et al., 2019). Each configuration is ran with 5 different seeds to be able to estimate its variance. A description of the hyper-parameter search and samples of our best models can be seen in B & C. For *IODINE* (Greff et al., 2019), we make use of the official trained model released by the authors.

Notation In reporting our results we will break down the results obtained in terms of the structure that was incorporated in the generator. We will denote *k*-GAN to describe a generator consisting of $K = k$ components, *k*-GAN *rel.* if it incorporates relational structure and *k*-GAN *ind.* if it does not. Additionally, we will append “bg.” when the model includes a separate background generator. We will use *k*-GAN to refer more generally to GANs that incorporate any of the proposed structure, and *GAN* to refer to the collection of GANs with different hyperparameters in our baseline.

5.1 QUALITATIVE ANALYSIS

Utilizing Structure We begin by analyzing the output of each (object) generator for *k*-GAN. Among the best performing models in our search, we consistently find that the final image is generated as a composition of images consisting of individual objects and background. It can be seen that in the process of learning to generate images, *k*-GAN learns about what are individual objects, and what is the background, without relying on prior knowledge or conditioning. Using this learned knowledge suggests a natural approach to unsupervised instance segmentation, which we shall explore later. Examples generated by *k*-GAN for each dataset can be seen in Figure 3 and Figure 4.

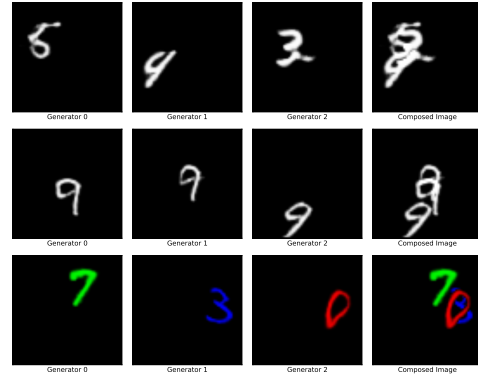


Figure 3: Generated images by 3-GAN on Multi-MNIST: *Independent* (top), *Triplet* (middle), and *RGB Occluded* (bottom). The three columns on the left show the output of each object generator, and the right column the composed image.

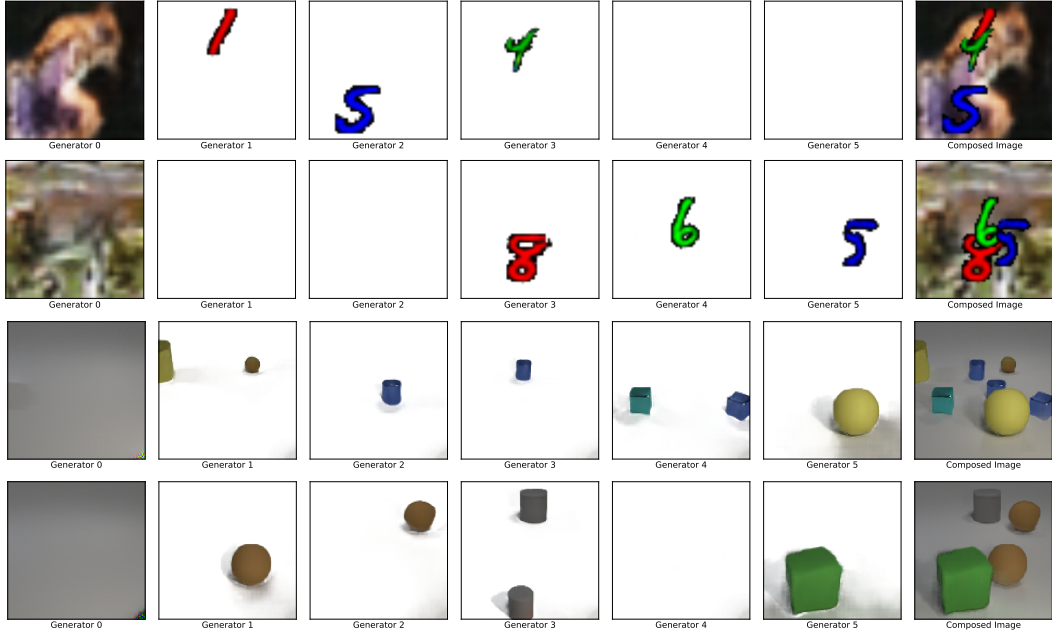


Figure 4: Generated samples by *5-GAN rel. bg.* on *CIFAR10 + MM* (top), and *CLEVR* (bottom). The left column corresponds to the output of the background generator. The next five columns are the outputs of each object generator, and the right column the composed image. Images are displayed as RGBA, with white denoting an alpha value of zero.

On *CLEVR*, where images often have a greater number of objects than the number of components K that was used during training, we find that the generator continues to learn a factored solution (i.e. using visual primitives that consist of 1-3 objects). This is interesting, as it suggests that using compositionality is preferable even when the factorization is sub-optimal. A similar tendency was found when analyzing generated images by *k-GAN ind.* when $k > 3$ on Multi-MNIST. The generator decodes some latents as “no digit” in attempting to generate the correct number of digits.

From the generated samples by *k-GAN rel.*, we observe that relations among the objects are correctly captured in most cases and that the relational mechanism can be used to generate the correct number of digits when K is greater than the number of objects in the dataset. We also observe that sometimes the background generator generates a *single* object together with the background. It rarely generates more than one object, which is further evidence that it is indeed more efficient to use the object generators.



Figure 5: Generated images by *5-GAN rel. bg.* (top) and *GAN* (bottom), when traversing the latent space of a single (object) generator. For *k-GAN* only a single digit is transformed, while for *GAN* the entire scene changes.



Figure 6: The best FID obtained by *GAN* and *k-GAN* on all datasets following our grid search. The best configurations were chosen based on the smallest average FID (across 5 seeds). Standard deviations across seeds are illustrated with error bars. For *IODINE* we made use of the official trained model for CLEVR released by the authors (Greff et al., 2019).

Latent Traversal We explore the degree to which the relational extension affects our initial independence assumption about objects. If it were to cause the latent representations to become fully dependent on one another then it could negate the benefits of compositionality. We conduct an experiment in which we traverse the latent space of a single latent vector in *k-GAN rel.* by adding a random vector to the original sample with fixed increments, and generate images from the resulting latent vectors. An example can be seen in Figure 5 (top), where we find that traversing the latent space of a single component affects only the green digit, whereas the visual presentation of the others remains unaffected.

We observe this behavior (i.e. the relational mechanism does not unnecessarily interfere) for the majority of the generated samples, confirming to a large degree our own intuition of how the relational mechanism should be utilized. When traversing the latent space of *GAN*, for which information about different objects is entangled, it results in a completely different scene (see Figure 5 bottom). Hence, by disentangling the underlying representation it is more robust to common variations in image space.

5.2 QUANTITATIVE ANALYSIS

Fréchet Inception Distance (FID) We train *k-GAN* and *GAN* on each dataset and compare the FID of the models with the lowest average FID across seeds (Figure 6). On all datasets but *CLEVR*, we find that *k-GAN* compares better or similar to *GAN*, although typically by a small margin. Importantly, compared to the recent *IODINE* (Greff et al., 2019), which also incorporates architectural structure to facilitate object compositionality, we observe that *k-GAN* significantly outperforms.

An analysis, using different variations of *k-GAN*, leads to several interesting observations. On the relational datasets (Figure 9) it can be observed that the relational extension is important to obtain good performance, while it does not harm performance when no relations are present. Likewise, on the background datasets (Figures 10 & 11) we find that the background extension is important, although some mitigation is possible using the relational mechanism. Finally, we observe several small differences in FID when changing the number of object generators K . Surprisingly, we find that the lowest FID on *Independent MM* is obtained by *4-GAN* without relational structure, which by definition is unable to consistently generate 3 digits. It suggests that FID is unable to capture these properties of images (motivating our human study), and renders any subtle FID differences between *k-GAN* and *GAN* inconclusive.

Instance Segmentation We train a segmenter on data sampled from *3-GAN* by treating the output of each object generator as pixel-level segmentation labels for the generated image (a similar technique was explored in Spampinato et al. (2019) for motion segmentation in videos). Note that this labeled

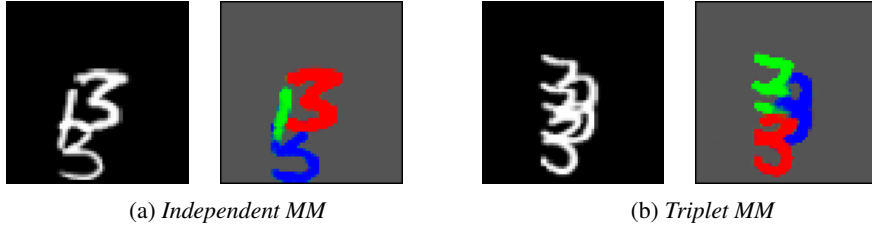


Figure 7: Result of segmenting unseen test-images using a segmenter that was trained on images (and labels) generated by 3-GAN. Note that this way of ‘inverting’ the learned generative model is only possible due to the added structure, which makes the generative process interpretable and semantically understood.

Dataset	Ground Truth	3-GAN
<i>Independent MM</i>	0.890	0.886 ± 0.003
<i>Triplet MM</i>	0.911	0.903 ± 0.002
<i>RGB Occluded MM</i>	0.928	0.955 ± 0.003
<i>CIFAR10 + MM</i>	0.950	0.814 ± 0.131

Table 1: ARI scores obtained by training a segmenter on *ground truth* data, and on samples from 3-GAN. Standard deviations are computed using generated data from the 5 best 3-GAN models according to FID.

data is obtained in a purely unsupervised fashion by exploiting the fact that, by incorporating structure, the learned generative process is now interpretable and semantically understood. We test how the segmenter generalizes to real images (Figure 7) for which we have ground-truth segmentations available and measure its accuracy using the Adjusted Rand Index (ARI) (Hubert & Arabie, 1985) score. We compare to training in purely supervised fashion on ground-truth data (further details are available in B).

In Table 1 we find that using unsupervised data from 3-GAN is often as good as using ground-truth (and can even have a positive regularization effect). These results strengthen our initial findings that k -GAN reliably generates images as compositions of objects. Moreover, it presents a novel approach to unsupervised instance segmentation that does not rely on an “encoder”, but rather leverages the structure of the learned generative process to perform inference.

Human Evaluation We asked humans to compare the images generated by k -GAN *rel.* to our GAN baseline on *RGB Occluded MM*, *CIFAR10 + MM*, and *CLEVR*, using the configuration with a background generator for the last two datasets⁵. For each model, we select the 10 best hyperparameter configurations (lowest FID), from which we each generate 100 images. We asked up to three raters for each image and report the majority vote or “Equal” if no decision was reached.

Figure 8a reports the results when asking human raters to compare the visual quality of the generated images by k -GAN to those by GAN. It can be seen that k -GAN compares favorably across all datasets, and in particular on *RGB Occluded MM* and *CIFAR10 + MM* we observe large differences. We find that k -GAN performs better even when $k > 3$, which can be attributed to the relational mechanism, allowing all components to agree on the correct number of digits.

In a second study we asked humans to report specific properties of the generated images, a complete list of which can be found in B. Here our goal was to assess if the generated images by k -GAN are more faithful to the reference distribution, which is particularly important in the context of representation learning. The results on *RGB Occluded MM* are summarized in Figure 8b. It can be seen that k -GAN more frequently generates images that have the correct number of objects, number of digits, and that satisfy all properties simultaneously. The difference between the correct number of digits and the correct number of objects suggests that the generated objects are often not recognizable

⁵On *CLEVR* we instructed the raters to ignore visual implausibilities due to floating objects (for both k -GAN and GAN) that may arise due to the fixed order in (6) and measured this effect separately in Figure 13.

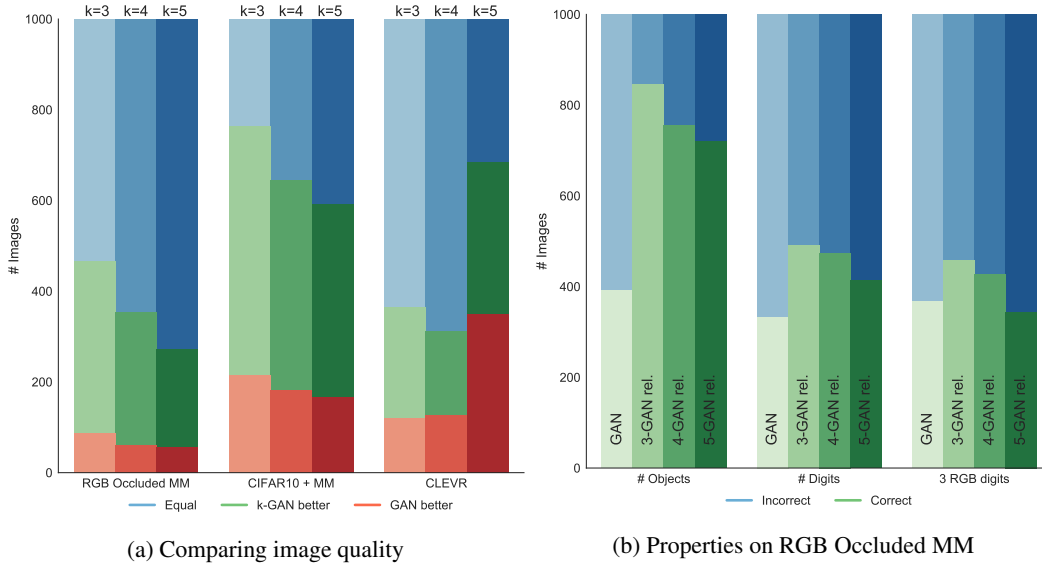


Figure 8: Results of human evaluation a) comparing the quality of the generated images by k -GAN ($k=3,4,5$) to GAN b) Properties of generated images by k -GAN ($k=3,4,5$) and GAN on *RGB Occluded MM*. It can be seen that k -GAN generates better images that are more faithful to the reference distribution.

as digits. This does not appear to be the case from the generated samples in **C**, suggesting that the raters may not have been familiar enough with the variety of MNIST digits.

On *CIFAR10 + MM* (Figure 12) it appears that GAN is able to accurately generate the correct number of objects, although the addition of background makes it difficult to provide a comparison in this case. Indeed, on the number of digits, k -GAN outperforms GAN by the same margin as one would expect compared to the results in Figure 8b.

Finally, in comparing the generated images by k -GAN and GAN on *CLEVR*, we noticed that the former generated more crowded scenes (containing multiple large objects in the center), and more frequently generated objects with distorted shapes or mixed colors. On the other hand, we found cases in which k -GAN generated scenes containing “flying” objects, a by-product of the fixed order in which we apply (6). We asked humans to score images based on these properties, which confirmed these observations (see Figure 13).

6 DISCUSSION

The experimental results confirm that the proposed structure is beneficial in generating images of multiple objects, and is utilized according to our own intuitions. By structuring the generative process, the generator learns about objects (and background) without requiring any supervision. Notably, we were able to extract this knowledge by ‘inverting’ the generative model to learn how to perform instance segmentation (and from which it is easy to obtain corresponding object representations). Indeed, although the computational complexity of our approach scales linearly with K (while the number of parameters stays constant due to sharing), these provide concrete reasons for why one would want to pursue this direction compared to other neural approaches to image generation and representation learning that do not incorporate structure.

In general, we find that it is encouraging to see that a simple inductive bias applied to standard neural network generator yields state of the art image generation capabilities compared to other purely unsupervised object-centric approaches. Especially with similar approaches requiring a lot more engineering to achieve worse results (Eslami et al., 2016; Greff et al., 2017; 2019). In that sense, it is likely that even better results can be obtained by building on the foundation as is presented here.

Conversely, we also expect that some of the innovations used here, such as a separate background generator, a relational mechanism, and compositing can be used to improve other approaches.

In order to benefit maximally from the presented structure, it is desirable to be able to accurately estimate the (minimum) number of objects in the images in advance. This task is ill-posed as it relies on a precise definition of “object” that is generally not available. In our experiments on *CLEVR* we encountered a similar situation in which the number of components used for training was often smaller than the number of objects in the images. Interestingly, we found that it does not render the incorporated structure meaningless, but that the generator discovers “primitives” that correspond to multiple objects as in Figure 4.

One area of improvement is in being able to accurately determine foreground, and background when combining the outputs of the object generators using alpha compositing. On *CLEVR* we observed cases in which objects appear to be flying, which is the result of being unable to route the information content of a “foreground” object to the corresponding “foreground” generator as induced by the fixed order in which images are composed. Although in principle the relational mechanism may account for this distinction, it may be easier to learn this when a more explicit mechanism is incorporated.

Another interesting avenue for improvement is to also incorporate structure in the discriminator, which acts as a loss function in the context of GANs. As we found that the pre-trained *Inception* embedding is limited in reasoning about the validity of multi-object images, the discriminator may experience similar difficulties in accurately judging images from being real or fake without additional structure. Ideally, we would have the discriminator reason about the correctness of each object individually, as well as the image as a whole. Adding additional ‘patch discriminators’ (Isola et al., 2017), where patches correspond to objects may serve a starting point in pursuing this direction.

7 CONCLUSION

We have investigated the usefulness (and the feasibility) of compositionality at the representational level of objects in GANs through a simple modification of a standard generator. The resulting *structured* GAN can be trained in a purely unsupervised manner as it does not rely on auxiliary inputs, and on a benchmark of multi-object datasets we have shown that our generative model learns about individual objects in the process of synthesizing samples. We have also shown how relations between objects, and background can be modeled by incorporating two modular extensions. A human study revealed that this leads to a better generative model of images compared to a strong baseline of GANs. Additionally, on the challenging *CLEVR* dataset (Johnson et al., 2017), it was shown how our approach is able to improve over IODINE (Greff et al., 2019) in terms of image generation capabilities, and a similar observation can be made for earlier purely unsupervised object-centric approaches, e.g. N-EM (Greff et al., 2017) or AIR (Eslami et al., 2016) by virtue of their inherent limitations.

The ultimate goal of this work is to learn structured generative models that can be inverted to perform representation learning. To this extent, we have proposed a novel approach to leverage the structure of the generator to generate data that can then be used to train an instance segmenter in a supervised fashion. We have shown that this segmenter generalizes to real images, which allows one to acquire corresponding object representations. By using GANs, we were able to overcome the limitations of other recent purely unsupervised object-centric approaches that do not scale to more complex multi-object images.

ACKNOWLEDGEMENTS

The authors wish to thank Damien Vincent, Alexander Kolesnikov, Olivier Bachem, Klaus Greff, and Paulo Rauber for helpful comments and constructive feedback. The authors are grateful to Marcin Michalski and Pierre Ruysen for their technical support. This research was in part supported by the Swiss National Science Foundation grant 200021_165675/1, and by hardware donations from NVIDIA Corporation as part of the Pioneers of AI Research award, and by IBM.

REFERENCES

- Relja Arandjelović and Andrew Zisserman. Object discovery with a copy-pasting gan. *arXiv preprint arXiv:1905.11369*, 2019.
- Martin Arjovsky, Soumith Chintala, and Léon Bottou. Wasserstein generative adversarial networks. In *International Conference on Machine Learning*, pp. 214–223, 2017.
- Samaneh Azadi, Deepak Pathak, Sayna Ebrahimi, and Trevor Darrell. Compositional gan: Learning image-conditional binary composition. *arXiv preprint arXiv:1807.07560*, 2019.
- Jimmy Lei Ba, Jamie Ryan Kiros, and Geoffrey E Hinton. Layer normalization. *arXiv preprint arXiv:1607.06450*, 2016.
- Peter W Battaglia, Jessica B Hamrick, and Joshua B Tenenbaum. Simulation as an engine of physical scene understanding. *Proceedings of the National Academy of Sciences*, pp. 201306572, 2013.
- Peter W Battaglia, Jessica B Hamrick, Victor Bapst, Alvaro Sanchez-Gonzalez, Vinicius Zambaldi, Mateusz Malinowski, Andrea Tacchetti, David Raposo, Adam Santoro, Ryan Faulkner, et al. Relational inductive biases, deep learning, and graph networks. *arXiv preprint arXiv:1806.01261*, 2018.
- Yoshua Bengio, Aaron Courville, and Pascal Vincent. Representation learning: A review and new perspectives. *IEEE transactions on pattern analysis and machine intelligence*, 35(8):1798–1828, 2013.
- Adam Bielski and Paolo Favaro. Emergence of object segmentation in perturbed generative models. In *Advances in Neural Information Processing Systems 32*, pp. 7254–7264, 2019.
- Mickaël Chen, Thierry Artières, and Ludovic Denoyer. Unsupervised object segmentation by redrawing. In *Advances in Neural Information Processing Systems 32*, pp. 12705–12716, 2019.
- Xi Chen, Yan Duan, Rein Houthoofd, John Schulman, Ilya Sutskever, and Pieter Abbeel. Infogan: Interpretable representation learning by information maximizing generative adversarial nets. In *Advances in neural information processing systems*, pp. 2172–2180, 2016.
- Laurent Dinh, Jascha Sohl-Dickstein, and Samy Bengio. Density estimation using real nvp. In *Fifth International Conference on Learning Representations, ICLR*, 2017.
- Jeff Donahue, Philipp Krähenbühl, and Trevor Darrell. Adversarial feature learning. In *Fifth International Conference on Learning Representations, ICLR*, 2017.
- Vincent Dumoulin, Ishmael Belghazi, Ben Poole, Olivier Mastropietro, Alex Lamb, Martin Arjovsky, and Aaron Courville. Adversarially learned inference. In *Fifth International Conference on Learning Representations, ICLR*, 2017.
- SM Ali Eslami, Nicolas Heess, Theophane Weber, Yuval Tassa, David Szepesvari, Geoffrey E Hinton, et al. Attend, infer, repeat: Fast scene understanding with generative models. In *Advances in Neural Information Processing Systems*, pp. 3225–3233, 2016.
- Ian Goodfellow, Jean Pouget-Abadie, Mehdi Mirza, Bing Xu, David Warde-Farley, Sherjil Ozair, Aaron Courville, and Yoshua Bengio. Generative adversarial nets. In *Advances in neural information processing systems*, pp. 2672–2680, 2014.
- Klaus Greff, Antti Rasmus, Mathias Berglund, Tele Hao, Harri Valpola, and Juergen Schmidhuber. Tagger: Deep unsupervised perceptual grouping. In *Advances in Neural Information Processing Systems*, pp. 4484–4492, 2016.
- Klaus Greff, Sjoerd van Steenkiste, and Jürgen Schmidhuber. Neural expectation maximization. In *Advances in Neural Information Processing Systems*, pp. 6691–6701, 2017.
- Klaus Greff, Raphaël Lopez Kaufman, Rishabh Kabra, Nick Watters, Christopher Burgess, Daniel Zoran, Loic Matthey, Matthew Botvinick, and Alexander Lerchner. Multi-object representation learning with iterative variational inference. In *International Conference on Machine Learning*, pp. 2424–2433, 2019.

- Karol Gregor, Ivo Danihelka, Alex Graves, Danilo Rezende, and Daan Wierstra. Draw: A recurrent neural network for image generation. In *International Conference on Machine Learning*, pp. 1462–1471, 2015.
- Ishaan Gulrajani, Faruk Ahmed, Martin Arjovsky, Vincent Dumoulin, and Aaron C Courville. Improved training of wasserstein gans. In *Advances in Neural Information Processing Systems*, pp. 5767–5777, 2017.
- Martin Heusel, Hubert Ramsauer, Thomas Unterthiner, Bernhard Nessler, and Sepp Hochreiter. Gans trained by a two time-scale update rule converge to a local nash equilibrium. In *Advances in Neural Information Processing Systems*, pp. 6626–6637, 2017.
- Irina Higgins, Loic Matthey, Arka Pal, Christopher Burgess, Xavier Glorot, Matthew Botvinick, Shakir Mohamed, and Alexander Lerchner. beta-vae: Learning basic visual concepts with a constrained variational framework. In *Fifth International Conference on Learning Representations, ICLR*, 2017.
- Tobias Hinz, Stefan Heinrich, and Stefan Wermter. Generating multiple objects at spatially distinct locations. In *International Conference on Learning Representations*, 2019.
- Lawrence Hubert and Phipps Arabie. Comparing partitions. *Journal of classification*, 2(1):193–218, 1985.
- Daniel Jiwoong Im, Chris Dongjoo Kim, Hui Jiang, and Roland Memisevic. Generating images with recurrent adversarial networks. *arXiv preprint arXiv:1602.05110*, 2016.
- Phillip Isola, Jun-Yan Zhu, Tinghui Zhou, and Alexei A Efros. Image-to-image translation with conditional adversarial networks. In *2017 IEEE Conference on Computer Vision and Pattern Recognition (CVPR)*, pp. 5967–5976. IEEE, 2017.
- Michael Janner, Sergey Levine, William T. Freeman, Joshua B. Tenenbaum, Chelsea Finn, and Jiajun Wu. Reasoning about physical interactions with object-centric models. In *International Conference on Learning Representations*, 2019.
- Justin Johnson, Bharath Hariharan, Laurens van der Maaten, Li Fei-Fei, C Lawrence Zitnick, and Ross Girshick. Clevr: A diagnostic dataset for compositional language and elementary visual reasoning. In *Proceedings of the IEEE Conference on Computer Vision and Pattern Recognition*, pp. 2901–2910, 2017.
- Justin Johnson, Agrim Gupta, and Li Fei-Fei. Image generation from scene graphs. In *Proceedings of the IEEE Conference on Computer Vision and Pattern Recognition*, pp. 1219–1228, 2018.
- Diederik P Kingma and Jimmy Ba. Adam: A method for stochastic optimization. In *Third International Conference on Learning Representations, ICLR*, 2015.
- Diederik P Kingma and Max Welling. Stochastic gradient vb and the variational auto-encoder. In *Second International Conference on Learning Representations, ICLR*, 2014.
- Adam Kosior, Hyunjik Kim, Yee Whye Teh, and Ingmar Posner. Sequential attend, infer, repeat: Generative modelling of moving objects. In *Advances in Neural Information Processing Systems*, pp. 8606–8616, 2018.
- Alex Krizhevsky, Geoffrey Hinton, et al. Learning multiple layers of features from tiny images. Technical report, Citeseer, 2009.
- Karol Kurach, Mario Lučić, Xiaohua Zhai, Marcin Michalski, and Sylvain Gelly. A large-scale study on regularization and normalization in gans. In *International Conference on Machine Learning*, pp. 3581–3590, 2019.
- Hanock Kwak and Byoung-Tak Zhang. Generating images part by part with composite generative adversarial networks. *arXiv preprint arXiv:1607.05387*, 2016.
- Nicolas Le Roux, Nicolas Heess, Jamie Shotton, and John Winn. Learning a generative model of images by factoring appearance and shape. *Neural Computation*, 23(3):593–650, 2011.

- Yann LeCun, Léon Bottou, Yoshua Bengio, Patrick Haffner, et al. Gradient-based learning applied to document recognition. *Proceedings of the IEEE*, 86(11):2278–2324, 1998.
- Chen-Hsuan Lin, Ersin Yumer, Oliver Wang, Eli Shechtman, and Simon Lucey. St-gan: Spatial transformer generative adversarial networks for image compositing. In *Proceedings of the IEEE Conference on Computer Vision and Pattern Recognition*, pp. 9455–9464, 2018.
- Mario Lucic, Karol Kurach, Marcin Michalski, Sylvain Gelly, and Olivier Bousquet. Are gans created equal? a large-scale study. In *Advances in neural information processing systems*, pp. 700–709, 2018.
- Takeru Miyato, Toshiki Kataoka, Masanori Koyama, and Yuichi Yoshida. Spectral normalization for generative adversarial networks. In *International Conference on Learning Representations*, 2018.
- Charlie Nash, SM Ali Eslami, Chris Burgess, Irina Higgins, Daniel Zoran, Theophane Weber, and Peter Battaglia. The multi-entity variational autoencoder. *NIPS Workshop on Learning Disentangled Representations: from Perception to Control*, 2017.
- Alec Radford, Luke Metz, and Soumith Chintala. Unsupervised representation learning with deep convolutional generative adversarial networks. *arXiv preprint arXiv:1511.06434*, 2015.
- Adam Santoro, David Raposo, David G Barrett, Mateusz Malinowski, Razvan Pascanu, Peter Battaglia, and Timothy Lillicrap. A simple neural network module for relational reasoning. In *Advances in neural information processing systems*, pp. 4967–4976, 2017.
- J Schmidhuber. Making the world differentiable: On using fully recurrent self-supervised neural networks for dynamic reinforcement learning and planning in non-stationary environments. *Institut für Informatik, Technische Universität München. Technical Report FKI-126*, 90, 1990.
- Jürgen Schmidhuber. Learning factorial codes by predictability minimization. *Neural Computation*, 4(6):863–879, 1992.
- Jürgen Schmidhuber. Generative adversarial networks are special cases of artificial curiosity (1990) and also closely related to predictability minimization (1991). *Neural Networks*, 2020.
- C Spampinato, S Palazzo, P D’Oro, D Giordano, and M Shah. Adversarial framework for unsupervised learning of motion dynamics in videos. *International Journal of Computer Vision*, pp. 1–20, 2019.
- Elizabeth S Spelke and Katherine D Kinzler. Core knowledge. *Developmental science*, 10(1):89–96, 2007.
- Aaron Van Oord, Nal Kalchbrenner, and Koray Kavukcuoglu. Pixel recurrent neural networks. In *International Conference on Machine Learning*, pp. 1747–1756, 2016.
- Sjoerd van Steenkiste, Michael Chang, Klaus Greff, and Jürgen Schmidhuber. Relational neural expectation maximization: Unsupervised discovery of objects and their interactions. In *International Conference on Learning Representations*, 2018a.
- Sjoerd van Steenkiste, Karol Kurach, and Sylvain Gelly. A case for object compositionality in deep generative models of images. *NeurIPS Workshop on Modeling the Physical World: Learning, Perception, and Control*, 2018b.
- Ashish Vaswani, Noam Shazeer, Niki Parmar, Jakob Uszkoreit, Llion Jones, Aidan N Gomez, Łukasz Kaiser, and Illia Polosukhin. Attention is all you need. In *Advances in Neural Information Processing Systems*, pp. 5998–6008, 2017.
- Kun Xu, Haoyu Liang, Jun Zhu, Hang Su, and Bo Zhang. Deep structured generative models. *arXiv preprint arXiv:1807.03877*, 2018.
- Jianwei Yang, Anitha Kannan, Dhruv Batra, and Devi Parikh. Lr-gan: Layered recursive generative adversarial networks for image generation. In *Fifth International Conference on Learning Representations, ICLR*, 2017.

Vinicius Zambaldi, David Raposo, Adam Santoro, Victor Bapst, Yujia Li, Igor Babuschkin, Karl Tuyls, David Reichert, Timothy Lillicrap, Edward Lockhart, Murray Shanahan, Victoria Langston, Razvan Pascanu, Matthew Botvinick, Oriol Vinyals, and Peter Battaglia. Deep reinforcement learning with relational inductive biases. In *International Conference on Learning Representations*, 2019.

A ADDITIONAL EXPERIMENT RESULTS

A.1 FID STUDY

Figures 9–11 and Table 2.

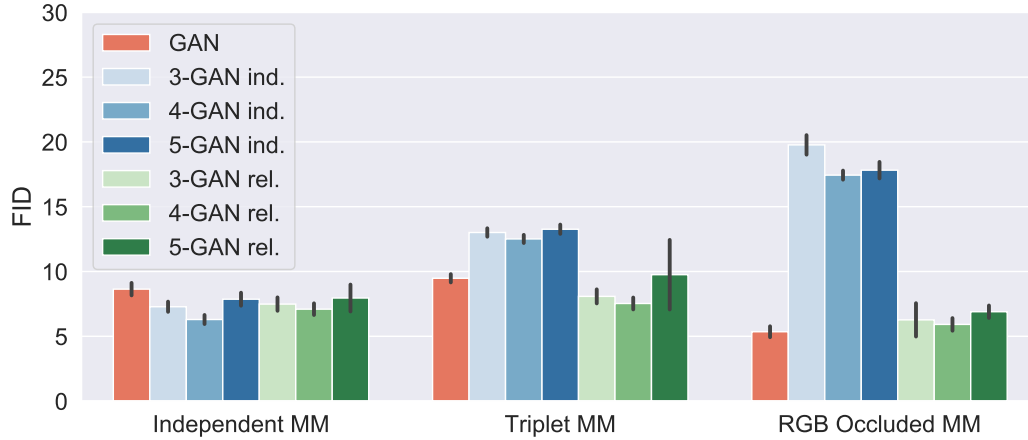


Figure 9: **Analysis.** The best FID obtained by *GAN* and *k-GAN* on *Independent MM*, *Triplet MM*, and *RGB Occluded MM* following our grid search. The best configurations were chosen based on the smallest average FID (across 5 seeds). Standard deviations across seeds are illustrated with error bars.

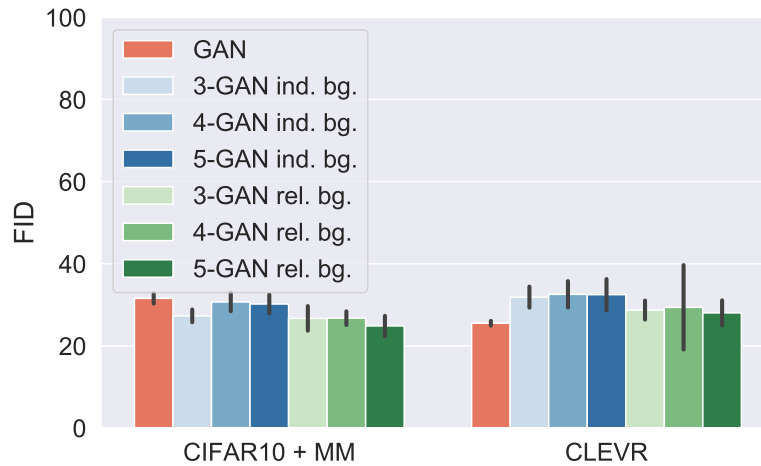


Figure 10: **Analysis.** The best FID obtained by *GAN* and *k-GAN* on *MM + CIFAR10*, and *CLEVR* following our grid search. In this figure all *k-GAN* variations make use of the background extension. The best configurations were chosen based on the smallest average FID (across 5 seeds). Standard deviations across seeds are illustrated with error bars.

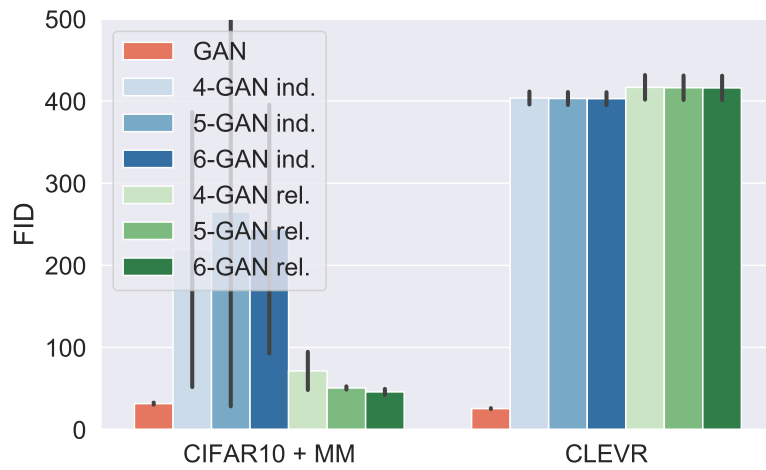


Figure 11: **Analysis.** The best FID obtained by *GAN* and *k-GAN* on *MM + CIFAR10*, and *CLEVR* following our grid search. In this figure all *k-GAN* variations do not use the background extension. The best configurations were chosen based on the smallest average FID (across 5 seeds). Standard deviations across seeds are illustrated with error bars.

model	gan type	norm.	penalty	blocks	heads	share	bg. int.	β_1	β_2	λ
GAN	NS-GAN	spec.	none	x	x	x	x	0.5	0.999	10
3-GAN ind.	NS-GAN	spec.	WGAN	x	x	x	x	0.9	0.999	1
4-GAN ind.	NS-GAN	spec.	WGAN	x	x	x	x	0.9	0.999	1
5-GAN ind.	NS-GAN	spec.	WGAN	x	x	x	x	0.9	0.999	1
3-GAN rel.	NS-GAN	spec.	WGAN	1	1	no	x	0.9	0.999	1
4-GAN rel.	NS-GAN	spec.	WGAN	1	1	no	x	0.9	0.999	1
5-GAN rel.	NS-GAN	spec.	WGAN	2	1	no	x	0.9	0.999	1
GAN	NS-GAN	spec.	none	x	x	x	x	0.5	0.999	1
3-GAN ind.	NS-GAN	spec.	WGAN	x	x	x	x	0.9	0.999	1
4-GAN ind.	NS-GAN	spec.	WGAN	x	x	x	x	0.9	0.999	1
5-GAN ind.	NS-GAN	spec.	WGAN	x	x	x	x	0.9	0.999	1
3-GAN rel.	NS-GAN	spec.	WGAN	1	1	no	x	0.9	0.999	1
4-GAN rel.	NS-GAN	spec.	WGAN	1	2	no	x	0.9	0.999	1
5-GAN rel.	NS-GAN	spec.	WGAN	2	1	no	x	0.9	0.999	1
GAN	NS-GAN	spec.	none	x	x	x	x	0.5	0.999	1
3-GAN ind.	NS-GAN	spec.	WGAN	x	x	x	x	0.9	0.999	1
4-GAN ind.	NS-GAN	spec.	WGAN	x	x	x	x	0.9	0.999	1
5-GAN ind.	NS-GAN	spec.	WGAN	x	x	x	x	0.9	0.999	1
3-GAN rel.	NS-GAN	none	WGAN	2	2	yes	x	0.9	0.999	1
4-GAN rel.	NS-GAN	none	WGAN	2	2	no	x	0.9	0.999	1
5-GAN rel.	NS-GAN	none	WGAN	2	2	yes	x	0.9	0.999	1
GAN	NS-GAN	none	WGAN	x	x	x	x	0.9	0.999	1
3-GAN ind. bg.	NS-GAN	none	WGAN	x	x	x	x	0.9	0.999	1
4-GAN ind. bg.	NS-GAN	none	WGAN	x	x	x	x	0.9	0.999	1
5-GAN ind. bg.	NS-GAN	none	WGAN	x	x	x	x	0.9	0.999	1
3-GAN rel. bg.	NS-GAN	none	WGAN	2	1	yes	yes	0.9	0.999	1
4-GAN rel. bg.	NS-GAN	none	WGAN	2	1	yes	yes	0.9	0.999	1
5-GAN rel. bg.	NS-GAN	none	WGAN	2	2	yes	no	0.9	0.999	1
GAN	WGAN	none	WGAN	x	x	x	x	0.9	0.999	1
3-GAN ind. bg.	NS-GAN	none	WGAN	x	x	x	x	0.9	0.999	1
4-GAN ind. bg.	NS-GAN	none	WGAN	x	x	x	x	0.9	0.999	1
5-GAN ind. bg.	NS-GAN	none	WGAN	x	x	x	x	0.9	0.999	1
3-GAN rel. bg.	NS-GAN	none	WGAN	2	1	no	yes	0.9	0.999	1
4-GAN rel. bg.	NS-GAN	none	WGAN	1	2	no	no	0.9	0.999	1
5-GAN rel. bg.	NS-GAN	none	WGAN	2	2	no	no	0.9	0.999	1

Table 2: best hyper-parameter configuration for each model that were obtained following our grid search. Configurations were chosen based on the smallest average FID (across 5 seeds) as reported in Figure 6. Each block corresponds to a dataset (from top to bottom: *Independent MM*, *Triplet MM*, *RGB Occluded MM*, *CIFAR10 + MM*, *CLEVR*).

A.2 HUMAN STUDY PROPERTIES

Figures 12–14.

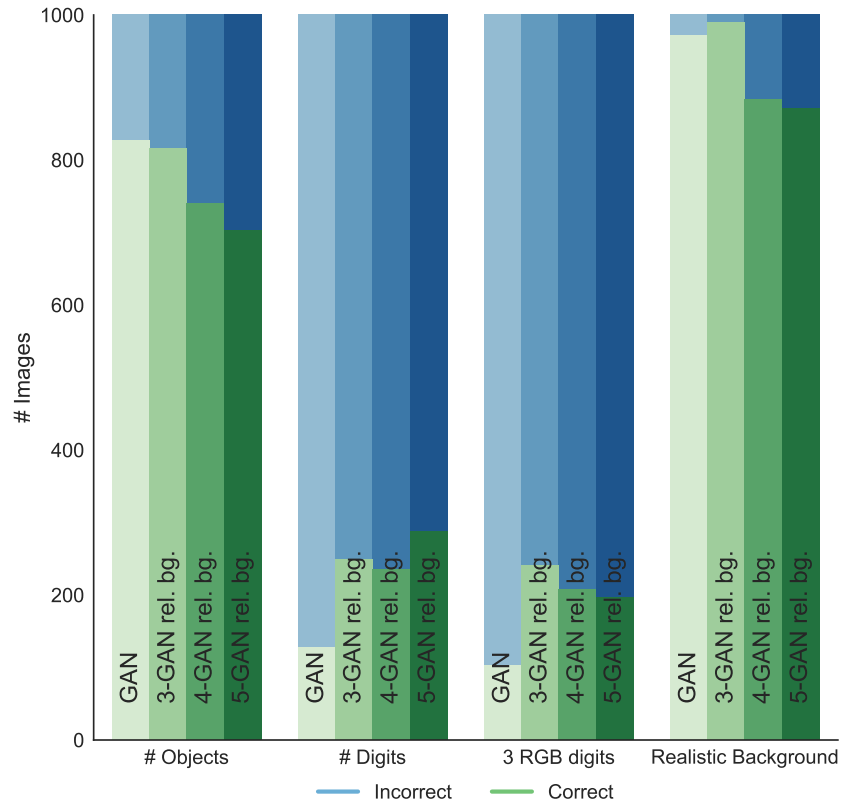


Figure 12: Additional results of human evaluation. Properties of generated images by k -GAN ($k=3,4,5$) and GAN on *CIFAR10* + *MM*.

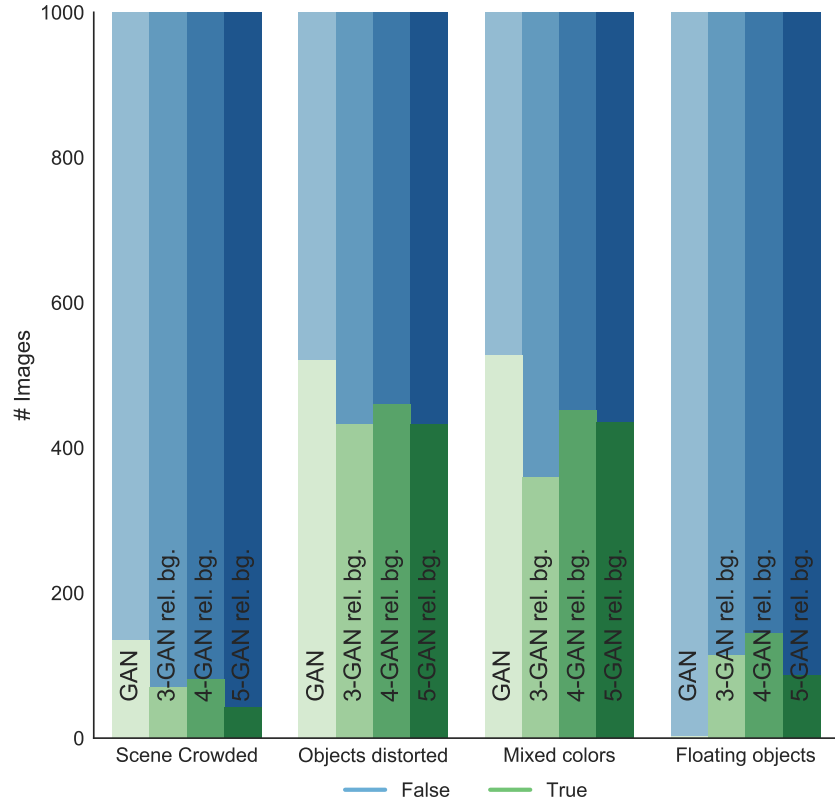


Figure 13: Additional results of human evaluation. Properties of generated images by k -GAN ($k=3,4,5$) and GAN on CLEVR. Note that on CLEVR all evaluated properties are undesirable, and thus a larger number of “False” responses is better.

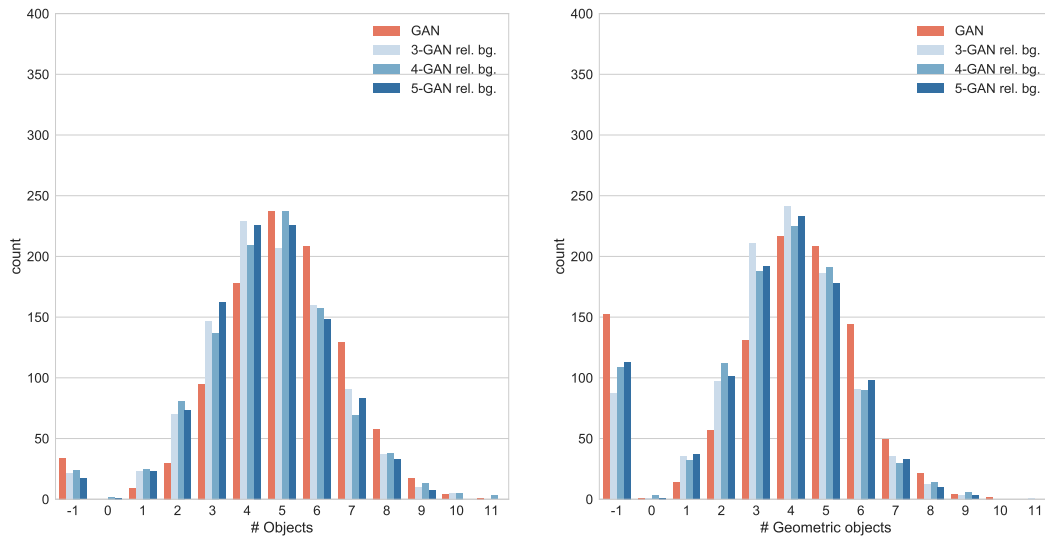


Figure 14: Results of human evaluation. Number of (geometric) objects in generated images by k -GAN ($k=3,4,5$) and GAN on CLEVR. A value of -1 implies a majority vote could not be reached.

B EXPERIMENT DETAILS

B.1 MODEL SPECIFICATIONS

The generator and discriminator neural network architectures in all our experiments are based on DCGAN (Radford et al., 2015).

Object Generators *k*-GAN *ind.* introduces $K = k$ copies of an object generator (i.e. tied weights, DCGAN architecture) that each generate an image from an independent sample of a 64-dimensional $UNIFORM(-1, 1)$ prior $P(Z)$.

Relational Structure When a relational stage is incorporated (*k*-GAN *rel.*) each of the $z_i \sim P(Z)$ is first updated, before being passed to the generators. These updates are computed using one or more *attention blocks*, which integrate Multi-Head Dot-Product Attention (MHDP) (Vaswani et al., 2017) with a post-processing step (Zambaldi et al., 2019). A single head of an attention block updates z_i according to (3), (4), and (5).

In our experiments, we use a single-layer neural network (fully-connected, 32 ReLU) followed by LayerNorm (Ba et al., 2016) for each of $MLP^{(q)}$, $MLP^{(k)}$, $MLP^{(v)}$. We implement $MLP^{(u)}$ with a two-layer neural network (each fully-connected, 64 ReLU), and apply LayerNorm after summing with z_i . Different heads in the same block use different parameters for $MLP^{(q)}$, $MLP^{(k)}$, $MLP^{(v)}$, $MLP^{(u)}$. If multiple heads are present, then their outputs are concatenated and transformed by a single-layer neural network (fully-connected, 64 ReLU) followed by LayerNorm to obtain the new \hat{z}_i . If the relational stage incorporates multiple attention blocks that iteratively update z_i , then we consider two variations: using unique weights for each MLP in each block or sharing their weights across blocks.

Background Generation When a background generator is incorporated (eg. *k*-GAN *rel. bg*) it uses the same DCGAN architecture as the object generators, yet maintains its own set of weights. It receives as input its own latent sample $z_b \sim P(Z_b)$, again using a $UNIFORM(-1, 1)$ prior, although one may in theory choose a different distribution. We explore both variations in which z_b participates in the relational stage, and in which it does not.

Composing On *Independent MM* and *Triplet MM* we sum the outputs of the object generators as in (2), followed by clipping to (0, 1). On all other datasets we use alpha compositing with a fixed order, i.e. using (6). In this case the object generators output an additional alpha channel, except for *RGB Occluded MM* in which we obtain alpha values by thresholding the output of each object generator at 0.1 for simplicity.

B.2 HYPERPARAMETER CONFIGURATIONS

Each model is optimized with ADAM (Kingma & Ba, 2015) using a learning rate of 0.0001, and batch size 64 for 1 000 000 steps. Each generator step is followed by 5 discriminator steps, as is considered best practice in training GANs. Checkpoints are saved at every 20 000th step and we consider only the checkpoint with the lowest FID for each hyper-parameter configuration. FID is computed using 10 000 samples from a hold-out set.

Baseline We conduct an extensive grid search over 48 different GAN configurations to obtain a strong GAN baseline on each dataset. It is made up of hyper-parameter ranges that were found to be successful in training GANs on standard datasets (Kurach et al., 2019).

We consider [SN-GAN / WGAN], using [NO / WGAN] gradient penalty with λ [1 / 10]. In addition, we consider these configurations [WITH / WITHOUT] spectral normalization. We consider [(0.5, 0.9) / (0.5, 0.999) / (0.9, 0.999)] as (β_1, β_2) in ADAM. We explore 5 different seeds for each configuration.

k-GAN We conduct a similar grid search for the GANs that incorporate our proposed structure. However, in order to maintain a similar computational budget compared to our baseline, we consider a *subset* of the previous ranges to compensate for the additional hyper-parameters of the different structured components that we would like to search over.

In particular, we consider SN-GAN with WGAN gradient penalty, with a default λ of 1, [WITH / WITHOUT] spectral normalization. We use (0.9, 0.999) as fixed values for (β_1, β_2) in ADAM. Additionally, we consider $K = [3 / 4 / 5]$ copies of the generator, and the following configurations for the relational structure:

- Independent
- Relational (1 block, no weight-sharing, 1 head)
- Relational (1 block, no weight-sharing, 2 heads)
- Relational (2 blocks, no weight-sharing, 1 head)
- Relational (2 blocks, weight-sharing, 1 head)
- Relational (2 blocks, no weight-sharing, 2 heads)
- Relational (2 blocks, weight-sharing, 2 heads)

This results in 42 hyper-parameter configurations, for which we each consider 5 seeds. We do not explore the use of a background generator on the non-background datasets. On the background datasets, we explore variations with and without the background generator. In the former case, we search over an additional hyper-parameter that determines whether the latent representation of the background generator should participate in the relational stage or not, while for the latter we increment all values of K by 1.

IODINE We made use of the official trained model for CLEVR released by the authors (Greff et al., 2019). We used $K = 7$ to compute the FID, which was also used for training. Lower values of K were considered but were not found to yield any improvements.

B.3 INSTANCE SEGMENTATION

We select the 5 best 3-GAN models (according to FID) on *Independent MM*, *Triplet MM*, *RGB Occluded MM*, *CIFAR10 + MM*. These include relational, and purely independent models, although on *CIFAR10 + MM* we ensure that we select only models that also incorporate the background extension. Segmentation data is obtained by either thresholding the output of the object generators at 0.1 (on *Independent MM*, *Triplet MM*) or using the (implicit) alpha masks (*RGB Occluded MM*, *CIFAR10 + MM*). Ground-truth data is obtained in the same fashion, but using the real images of digits and background before combining them.

Our segmentation architecture is similar to the one considered in Chen et al. (2019) but trained in a supervised fashion. We use a straight-through estimator that first considers all viable permutations of assigning segmentation outputs to labels, and then back-propagates only the gradients of the permutation for which we measure the lowest cross-entropy loss.

We test the trained segmenter on ground-truth data and report the Adjusted Rand Index (ARI) (Hubert & Arabie, 1985) score on all pixels that correspond to digits in line with prior work (Greff et al., 2017). On *Independent MM*, and *Triplet MM* we additionally ignore overlapping pixels due to ambiguities.

B.4 HUMAN STUDY

We asked human raters to compare the images generated by k -GAN ($k = 3, 4, 5$) to our GAN baseline on *RGB Occluded MM*, *CIFAR10 + MM* and *CLEVR*, using the configuration with a background generator for the last two datasets. For each model, we select the 10 best hyper-parameter configurations, from which we each generate 100 images. We conduct two different studies 1) in which we compare images from k -GAN against GAN and 2) in which we asked raters to answer questions about the content (properties) of the images.

Comparison We asked reviewers to compare the quality of the generated images. We asked up to three raters for each image and report the majority vote or “none” if no decision can be reached. Note that on *CLEVR* we instructed the raters to ignore visual implausibilities due to floating objects (for both k – GAN and GAN) that may arise due to the fixed order in (6), and measured this effect separately in Figure 13.

Properties For each dataset, we asked (up to three raters for each image) the following questions.

On *RGB Occluded MM* we asked:

1. How many [red, blue, green] shapes are in the image? Answers: [0, 1, 2, 3, 4, 5]
2. How many are recognizable as digits? Answers: [0, 1, 2, 3, 4, 5]
3. Are there exactly 3 digits in the picture, one of them green, one blue and one red? Answers: Yes / No

On *CIFAR10 + MM* we asked these same questions, and additionally asked:

4. Does the background constitute a realistic scene? Answers: Yes / No

On *CLEVR* we asked the following set of questions:

1. How many shapes are in the image? Answers: [0, 1, 2, 3, 4, 5, 6, 7, 8, 9, 10]
2. How many are recognizable as geometric objects? Answers: [0, 1, 2, 3, 4, 5, 6, 7, 8, 9, 10]
3. Are there any objects with mixed colors (eg. part green part red)? Answers: Yes / No
4. Are there any objects with distorted geometric shapes?: Answers: Yes / No
5. Are there any objects that appear to be floating? Answers: Yes / No
6. Does the scene appear to be crowded? Answers: Yes / No

C OVERVIEW OF REAL AND GENERATED SAMPLES

Generated samples (8×8 grid) are shown for the best (lowest FID) structured GAN following our grid search, as well as the best baseline GAN for each dataset. Real samples from the dataset can also be seen.

C.1 INDEPENDENT MULTI MNIST

Figures 15–17.

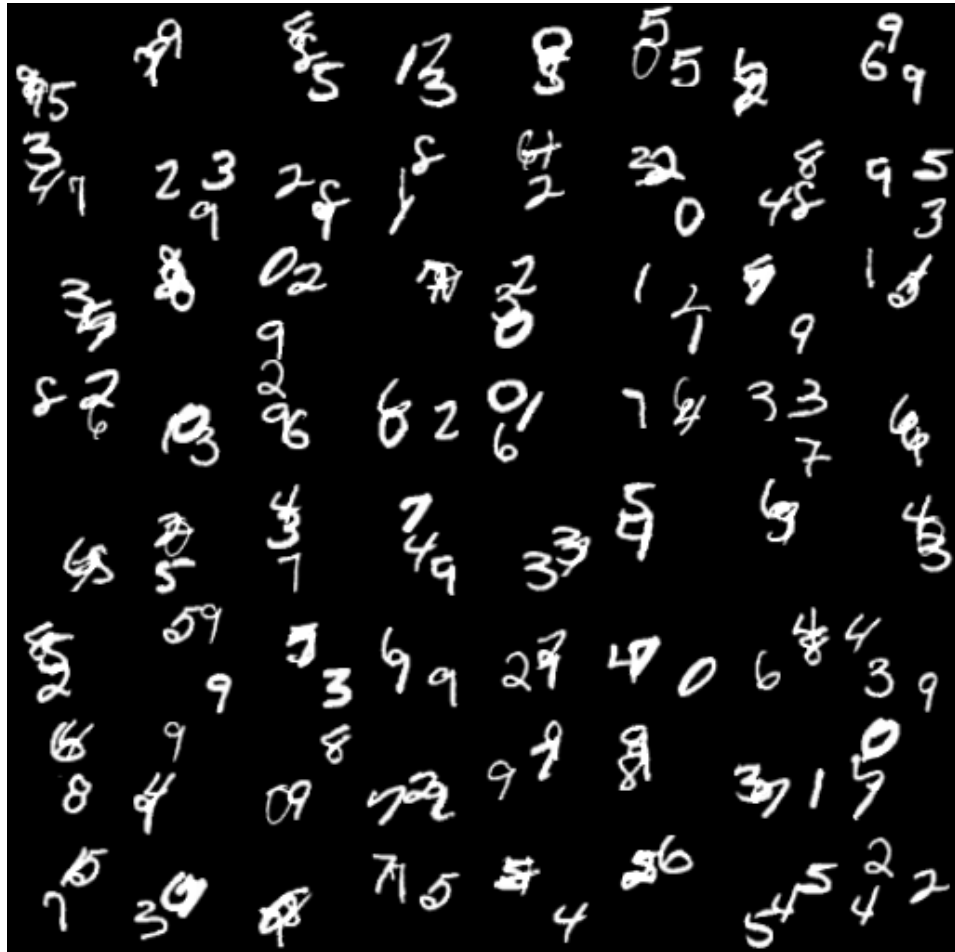


Figure 15: Real

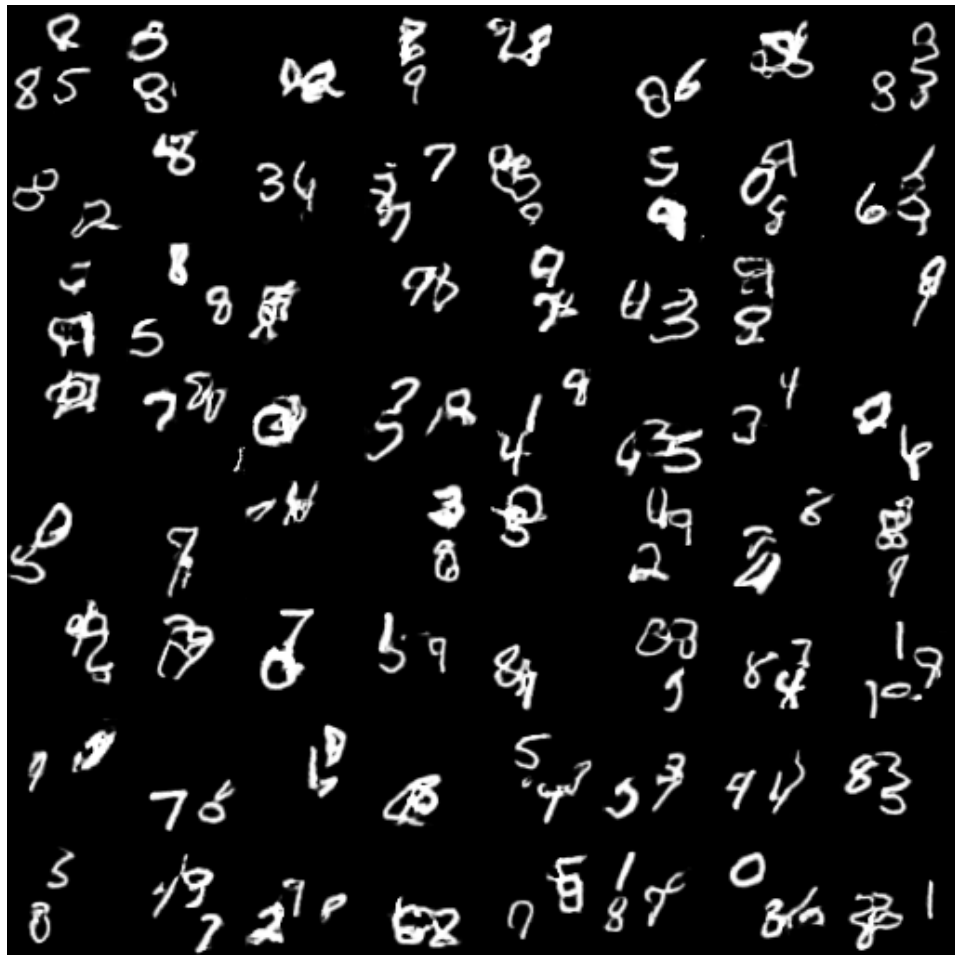


Figure 16: NS-GAN with spectral norm

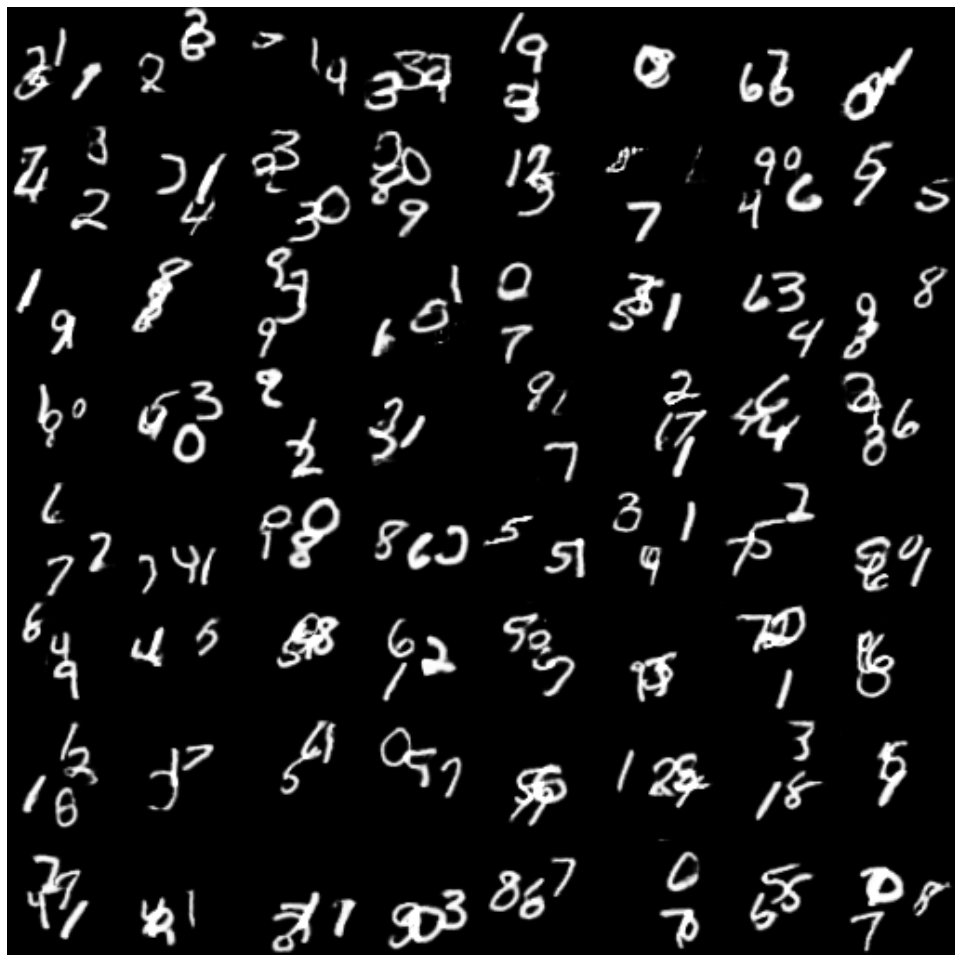


Figure 17: 4-GAN ind. with spectral norm and WGAN penalty

C.2 TRIPLET MULTI MNIST

Figures 18–20.

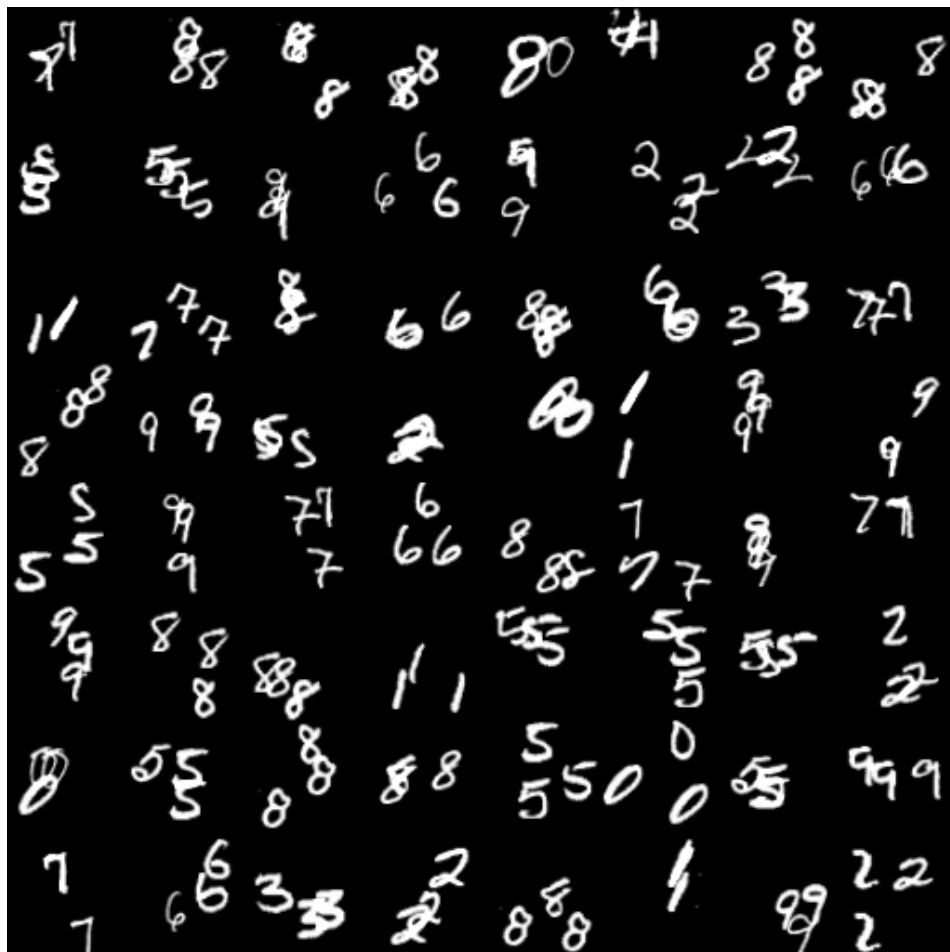


Figure 18: Real

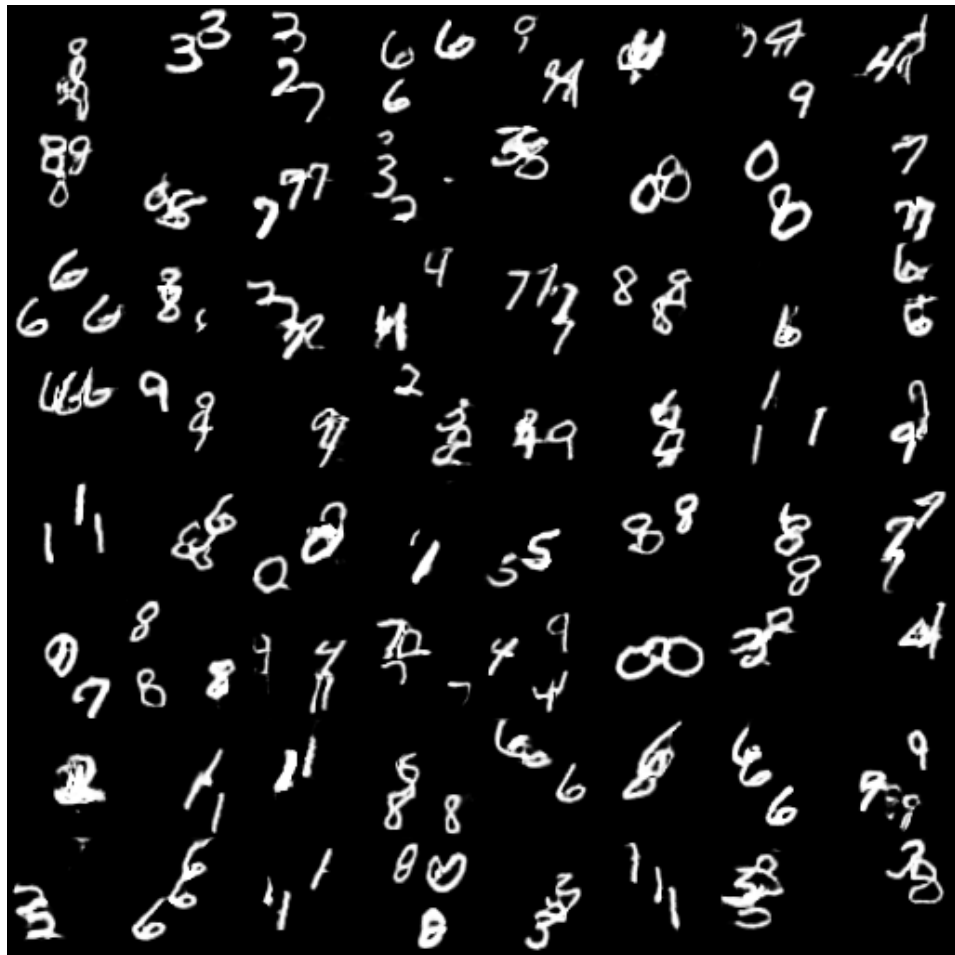


Figure 19: NS-GAN with spectral norm



Figure 20: 4-GAN rel. (1 block, 2 heads, no weight sharing) with spectral norm and WGAN penalty

C.3 RGB-OCCLUDED MULTI MNIST

Figures 21–23.

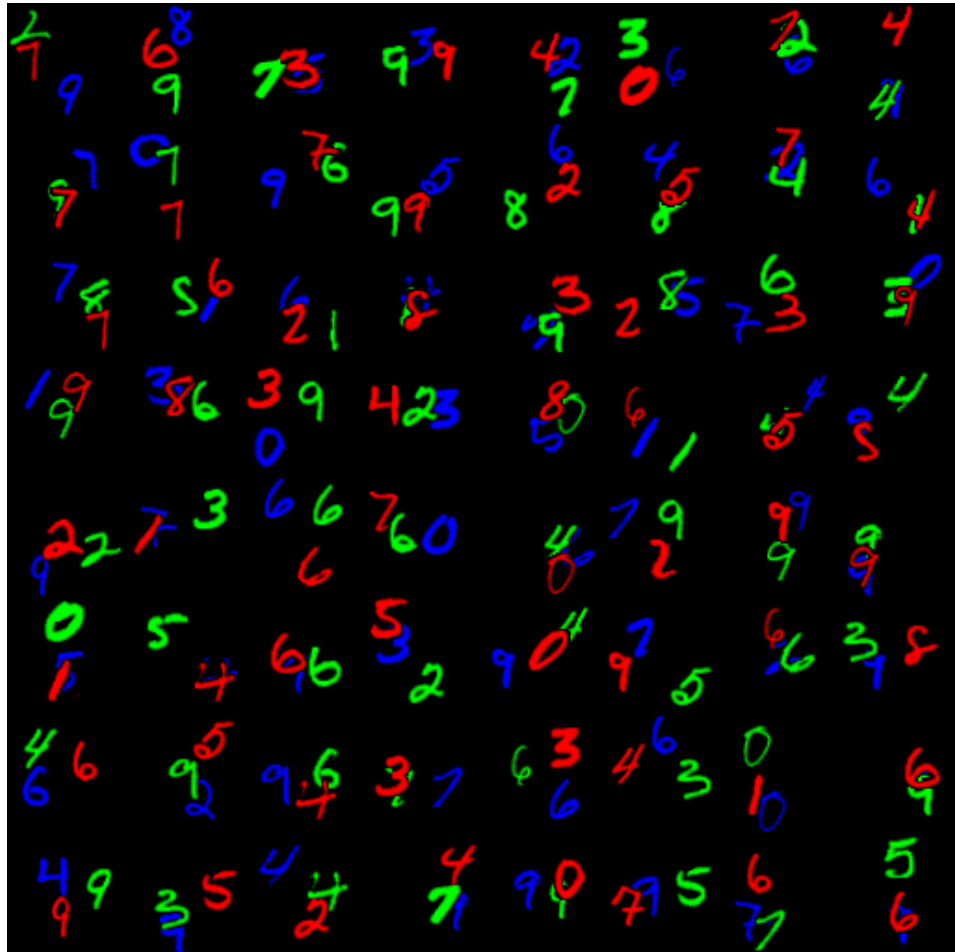


Figure 21: Real

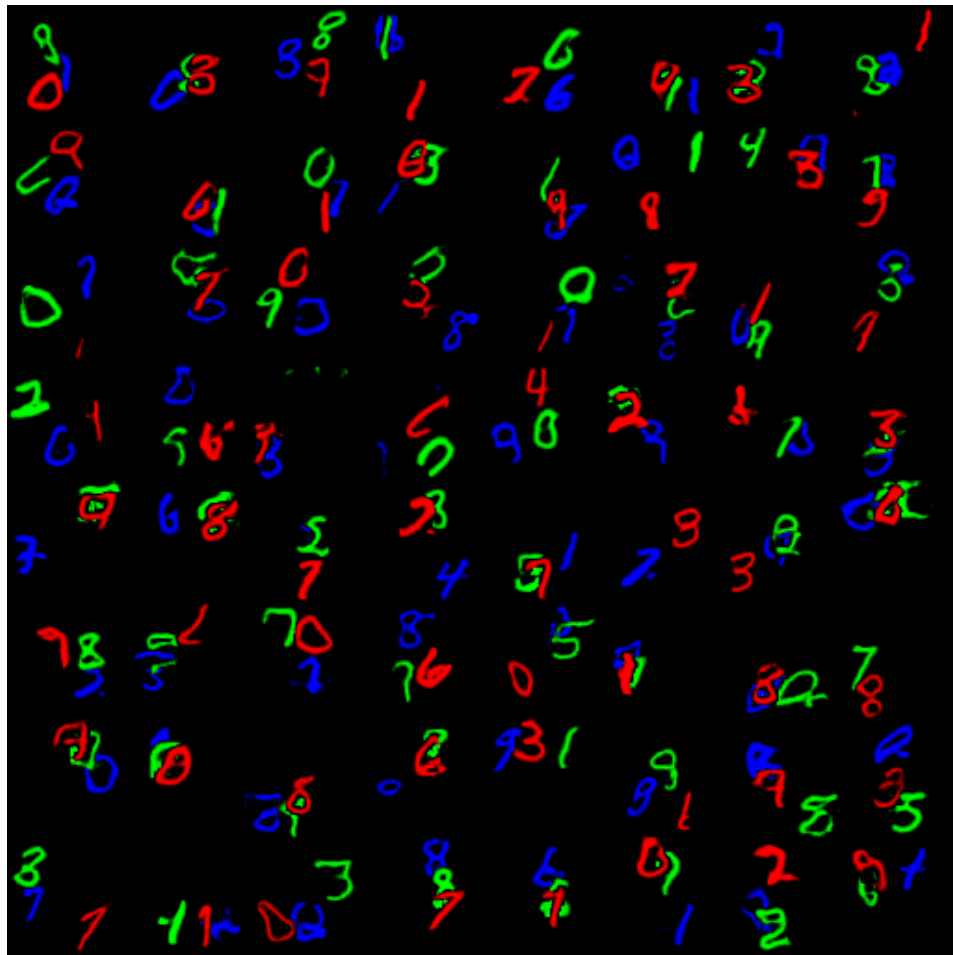


Figure 22: NS-GAN with spectral norm

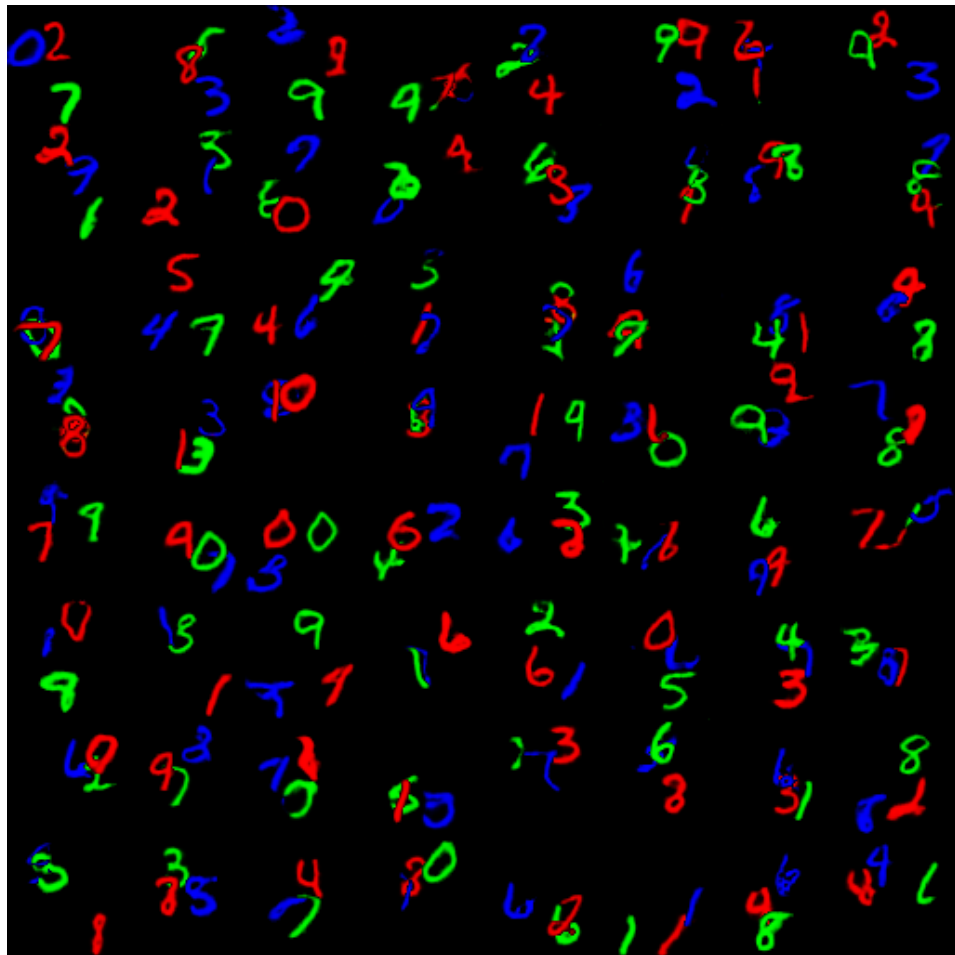


Figure 23: 3-GAN rel. (2 blocks, 2 heads, no weight sharing) with spectral norm and WGAN penalty

C.4 CIFAR10 + MM

Figures 24–26.

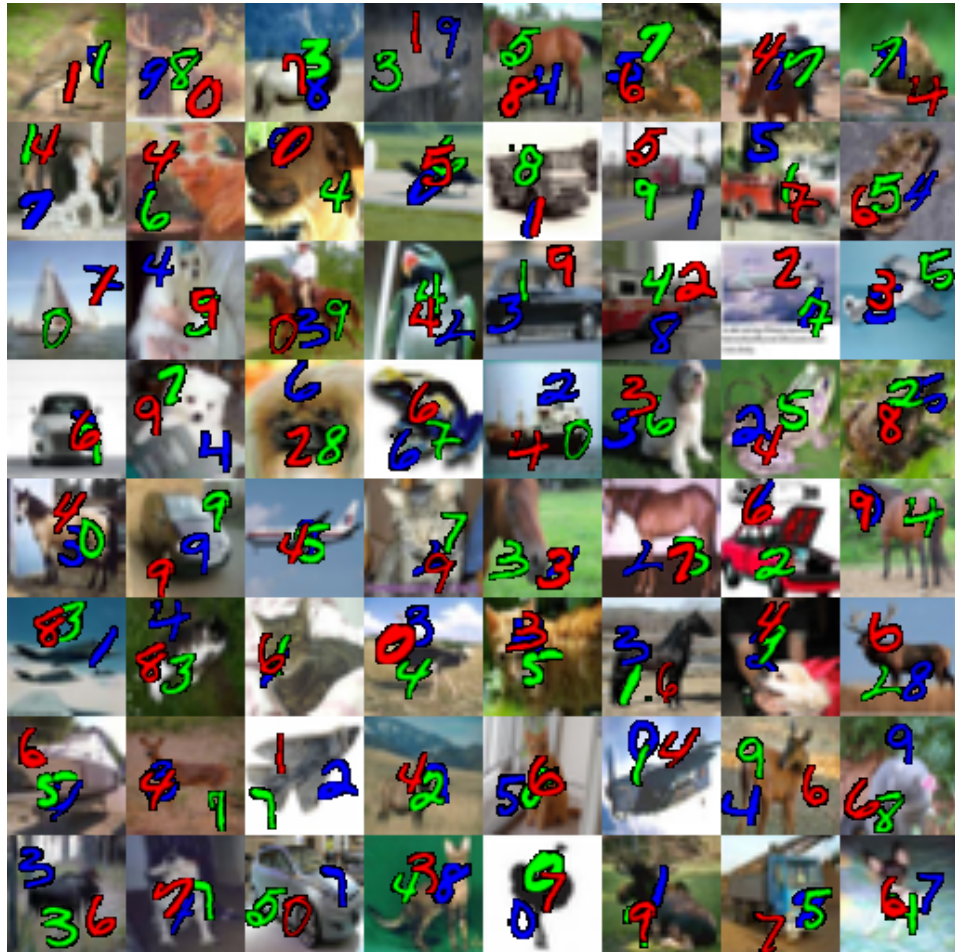


Figure 24: Real



Figure 25: WGAN with WGAN penalty

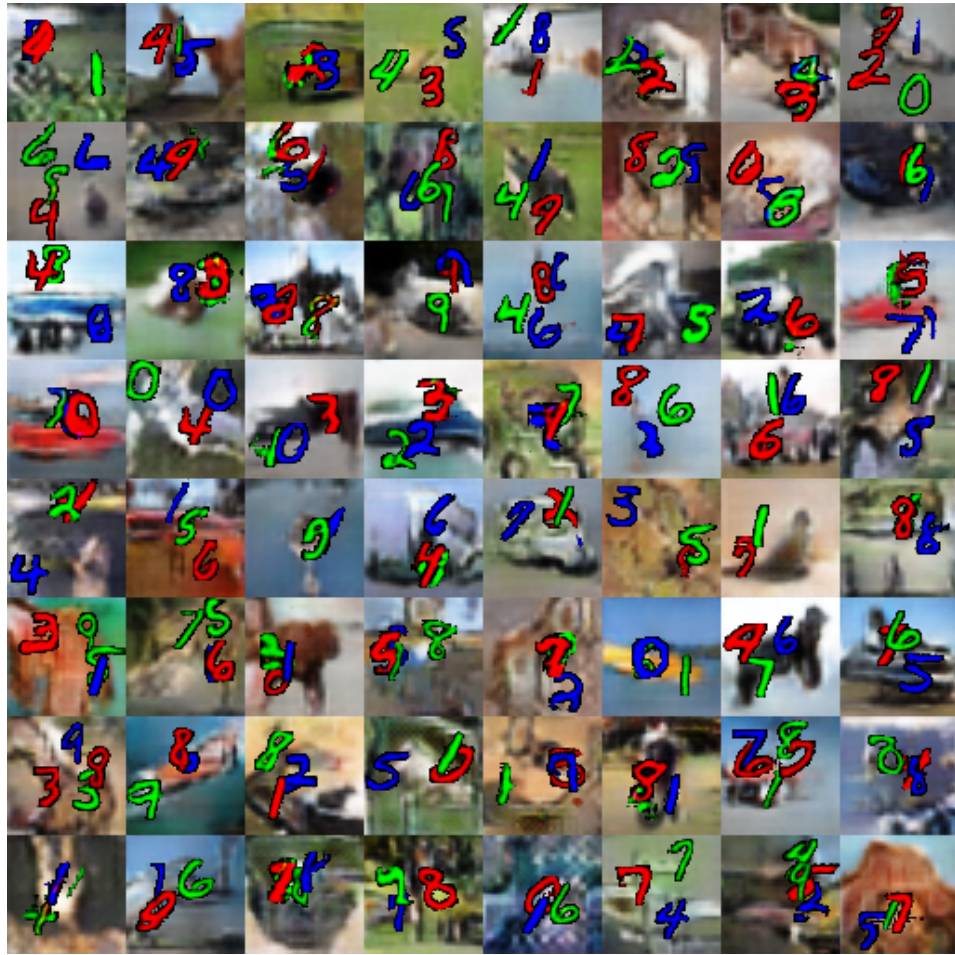


Figure 26: 5-GAN rel. (1 block, 2 heads, no weight sharing) bg. (no interaction) with WGAN penalty

C.5 CLEVR

Figures 27–29.

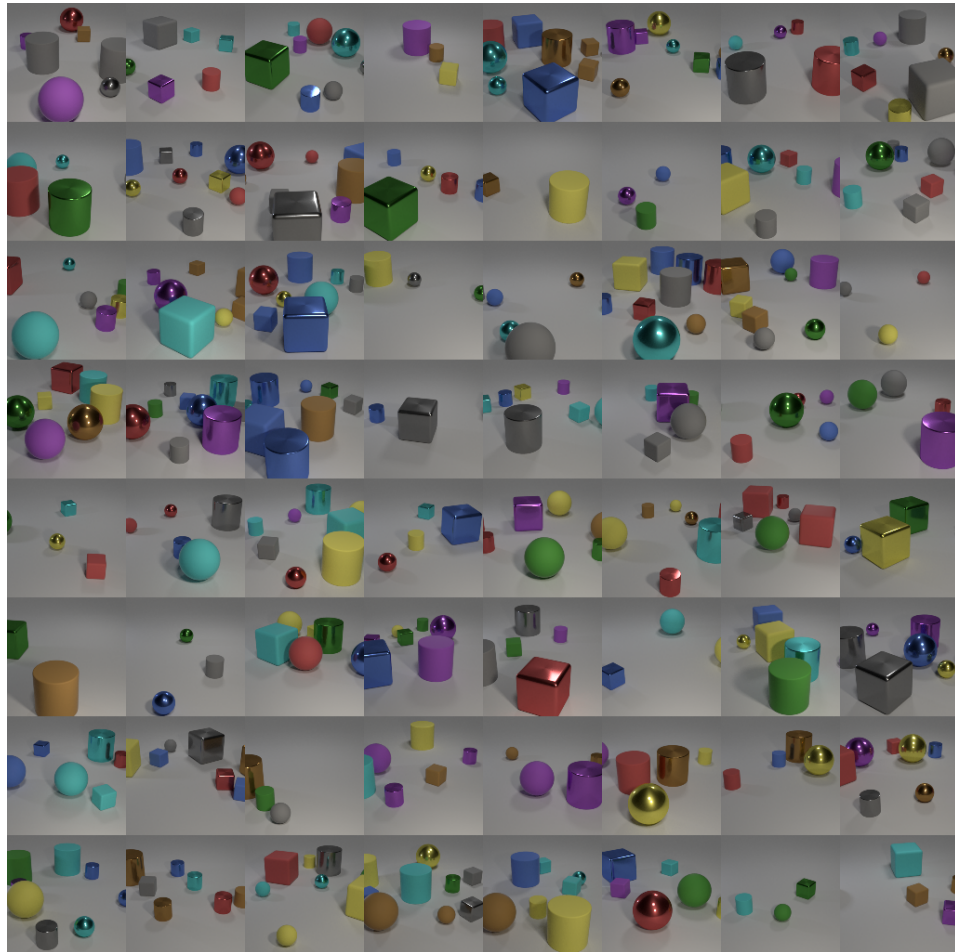


Figure 27: Real

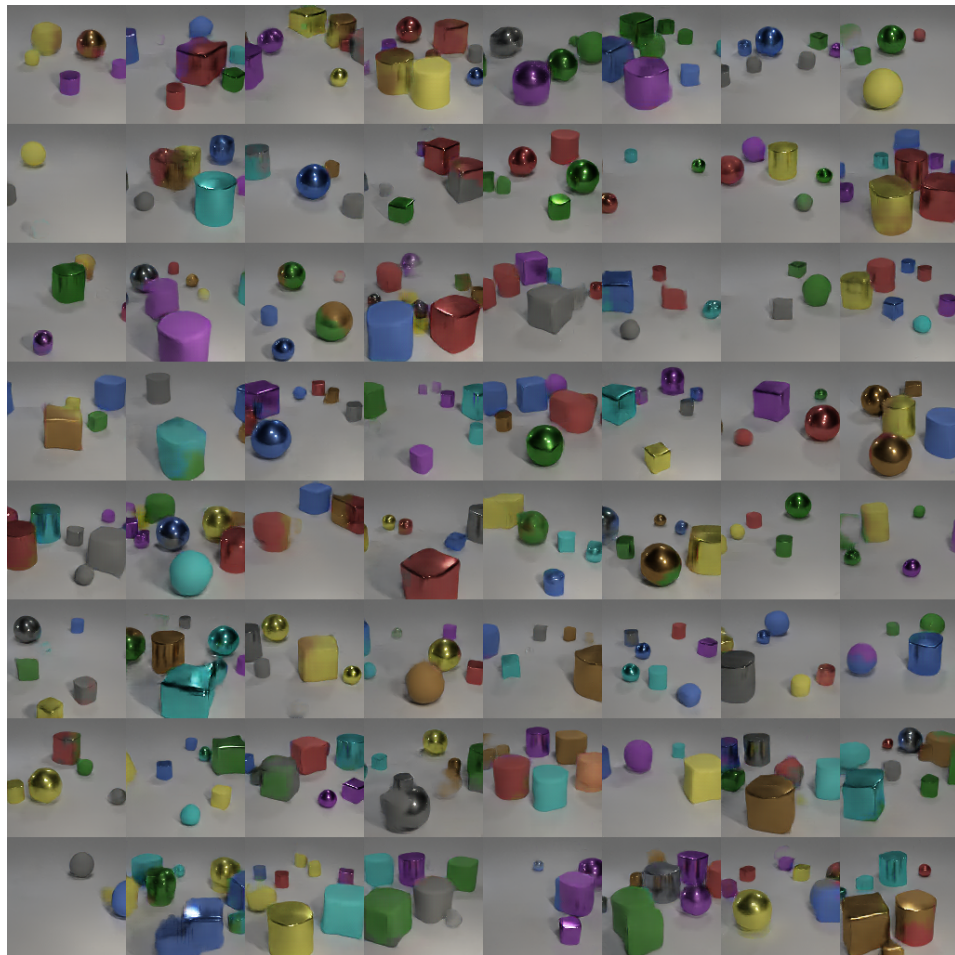


Figure 28: WGAN with WGAN penalty

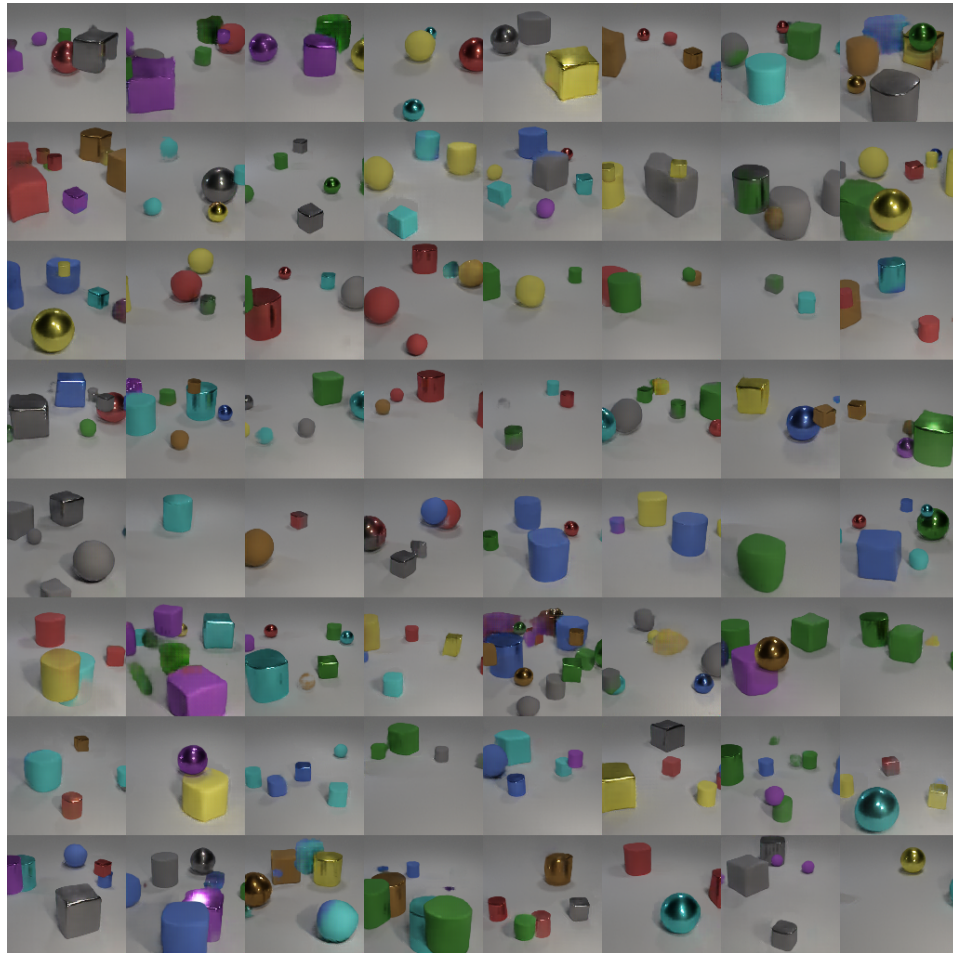


Figure 29: 3-GAN rel. (2 heads, 2 blocks, no weight sharing) bg. (with interaction) with WGAN penalty.